Supernarrow spectral peaks and high-frequency stochastic resonance in systems with coexisting periodic attractors

M. I. Dykman
Department of Physics, Stanford University, Stanford, California 94305

D. G. Luchinsky*
School of Physics and Materials, Lancaster University, Lancaster, LA1 4YB, United Kingdom.

R. Mannella
Dipartimento di Fisica, Università di Pisa, Piazza Torricelli 2, 56100 Pisa, Italy

P. V. E. McClintock, N. D. Stein, and N. G. Stocks†
School of Physics and Materials, Lancaster University, Lancaster, LA1 4YB, United Kingdom
(Received 14 July 1993)

The kinetics of a periodically driven nonlinear oscillator, bistable in a nearly resonant field, has been investigated theoretically and through analog experiments. An activation dependence of the probabilities of fluctuational transitions between the coexisting attractors has been observed, and the activation energies of the transitions have been calculated and measured for a wide range of parameters. The position of the kinetic phase transition (KPT), at which the populations of the attractors are equal, has been established. A range of critical phenomena is shown to arise in the vicinity of the KPT including, in particular, the appearance of a supernarrow peak in the spectral density of the fluctuations, and the occurrence of high-frequency stochastic resonance (HFSR). The experimental measurements of the transition probabilities, the KPT line, the multipeaked spectral densities, the strength of the supernarrow spectral peak, and the HFSR effect are shown to be in good agreement with the theoretical predictions.

PACS number(s): 05.40.+j, 02.50.−r

I. INTRODUCTION

Bistable systems are characterized both by local relaxation times t_{ri}, t_{rj} *about* their stable states i, j, and by reciprocal $i \to j$ transition probabilities W_{ij}^{-1} between them. Provided that

$$W_{ij}t_{ri}, \quad W_{ji}t_{rj} \ll 1 \tag{1}$$

the concept of bistability is meaningful, because a system will then spend most of the time fluctuating about one or other of the stable states. If its parameters pass through the range of bistability in a time much less than W_{ij}^{-1}, the system will display hysteresis: it will tend to remain within one or the other of the stable states, depending on the prior history. For fixed system parameters, however, over times $\sim W_{ij}^{-1}$ a stationary distribution over the stable states is built up and the system "forgets" which of the stable states was occupied initially.

The transition probabilities of thermal equilibrium systems are usually given by the Arrhenius law, $W \propto \exp(-E_a/T)$, where T is the temperature and E_a is the characteristic activation energy of the transition; in the case of a Brownian particle the quantity E_a is simply the depth of the potential well from which the particle escapes [1]. For nonequilibrium systems, however, the calculation of the transition probabilities is a nontrivial problem. A rather general approach to its solution has been proposed for dynamical systems driven by external Gaussian noise (see [2] for a review). In this case $W \propto \exp(-R/\alpha)$, where α is the noise intensity, while R is given by the solution of a certain variational problem.

In the general case of a bistable system, the characteristic activation energies R_1 and R_2 for the transitions $1 \to 2$ and $2 \to 1$ differ from one another. Consequently, for sufficiently weak noise, i.e., for small α [when (1) is fulfilled and in addition W is much smaller than the reciprocal correlation time of the noise], W_{12} and W_{21} differ exponentially. So also do the stationary populations w_1 and w_2 of the stable states,

$$w_1 = \frac{W_{21}}{W_{12}+W_{21}}, \qquad w_2 = \frac{W_{12}}{W_{12}+W_{21}}. \tag{2}$$

For most parameter values, the ratio w_1/w_2 is either exponentially small (for $R_2 - R_1 \gg \alpha$) or large (for $R_1 - R_2 \gg \alpha$) and the system occupies with an overwhelming probability the state 2 or 1, respectively. Only within a

*Permanent address: Research Institute for Metrological Service, 117965 Moscow, Russia.

†Present address: Department of Engineering, University of Warwick, Coventry, CV4 7AL, United Kingdom.

very narrow range of parameters where $|R_1 - R_2| \lesssim \alpha$ are the populations w_1 and w_2 of the same order of magnitude. In this range a kinetic phase transition occurs: as we discuss below, the behavior of a noise-driven dynamical system is to some extent analogous to that of a thermodynamic system with coexisting phases (e.g., liquid-vapor) within the range of its first-order phase transition, where both phases are well manifested (with comparable molar volumes, for example).

A well-known signature of systems experiencing phase transitions is the strong associated increase of fluctuations. It is quite natural to expect that the large occasional fluctuations between stable states (the analog of the fluctuational creation of macrobubbles in a liquid-vapor system) will give rise to intense and extremely narrow (with a width $\sim W$) peaks in the susceptibility of the system and in the spectral density of fluctuations (SDF) [3]. For a Brownian particle fluctuating in a symmetric double-well potential (that is, exactly at the phase-transition point, $w_1 = w_2$), the corresponding peak in the SDF at zero frequency has already been observed [4]. The exponentially fast broadening of this peak with increasing noise intensity gives rise [5] to low-frequency *stochastic resonance* [6–8], i.e., to the increase with increasing noise of the signal and the signal-to-noise ratio in a system driven by a low-frequency periodic force.

An important class of bistable systems is those that display bistability when driven by an intense periodic field, but which are monostable otherwise. (Note that some such systems may also display multistability, and/or dynamical chaos, when subjected to even stronger periodic fields.) A variety of them are investigated in, for example, nonlinear optics (in relation to optical bistability, see [9]). The different stable states here correspond to periodic attractors with differing amplitudes, phases (and sometimes frequencies) of constrained vibrations. One well-known example [10] of such a system, the single-well Duffing oscillator driven by a nearly resonant field, is interesting not only as an archetypal model for the investigation of a periodic-field induced bistability, but also because it refers directly to a peculiar and interesting physical system, a relativistic electron trapped in a magnetic field and excited by resonant cyclotron radiation [11].

In addition to its markedly nonequilibrium character, which provides a good test for theories of fluctuational transitions in thermally nonequilibrium systems, the model also enables one to investigate specific phenomena arising in systems with coexisting states of forced vibration within the range of the kinetic phase transition. Since there is a special frequency in such systems, namely, the frequency of the external field ω_F, the fluctuational transitions between the stable states should modulate the response of the system at frequency ω_F: extremely tall and narrow spectral peaks near ω_F are therefore to be expected, both in the susceptibility [2] and in the SDF [12]. Such supernarrow spectral peaks have been observed in an electronic analog experiment [13]. Because the widths of such peaks increase extremely rapidly (exponentially) with noise intensity, it is to be anticipated that the signal-to-noise ratio for a signal at a frequency close to ω_F will also increase with increasing noise intensity, i.e., that there will be a manifestation of high-frequency stochastic resonance (HFSR).

In the present paper we present detailed results of our investigation of the features of the SDF in a periodically driven system, including the onset of a supernarrow spectral peak in the region of the kinetic phase transition. In Sec. II the theory of kinetic phenomena for a periodically driven oscillator is given, including the results of a numerical calculation of the "activation energies" of the fluctuational transitions and explicit expressions for the spectral density of fluctuations and for the generalized susceptibilities. In Sec. III the experimental simulation of the oscillator by an analog electronic circuit is described. In Sec. IV the theoretical and experimental results are compared with each other, and the critical phenomena, the onset of the supernarrow spectral peak and of the high-frequency stochastic resonance, are discussed. Section V contains concluding remarks.

II. THEORY OF THE SPECTRAL DENSITY OF FLUCTUATIONS OF AN OSCILLATOR BISTABLE IN A PERIODIC FIELD

A. Model

In this section we explore the behavior of a nonlinear oscillator subject to the combined influences of a periodic field $F\cos\omega_F t$ and a weak random force $f(t)$. The equation of motion of the particular oscillator considered (single-well Duffing oscillator) is

$$\ddot{q} + 2\Gamma\dot{q} + \omega_0^2 q + \gamma q^3 = F\cos\omega_F t + f(t)\,. \tag{3}$$

The oscillator is assumed underdamped and the periodic field nearly resonant

$$\Gamma,\ |\delta\omega| \ll \omega_F, \qquad \delta\omega = \omega_F - \omega_0\,. \tag{4}$$

A characteristic amplitude of vibration for which the oscillator will obviously be strongly nonlinear, the nonlinear length l_n, is determined by the condition that the nonlinear term γq^3 in (3) should be as large as the linear one, so that $l_n = (\omega_0^2/|\gamma|)^{\frac{1}{2}}$. If the amplitude F of the periodic force is sufficiently large that vibrations of amplitude $a \sim l_n$ are excited, then the oscillator (3) in the absence of the random force $f(t)$ is known [14] to display deterministic chaotic phenomena (see also [15]), with the boundaries of the domains of attraction to various attractors often being fractal [16].

In the case of an underdamped oscillator, strong nonlinear effects can also arise for much smaller values of F, for which the vibration amplitudes a are correspondingly much less than l_n [10]. This is because the eigenfrequency of the vibrations of a nonlinear oscillator depends on their amplitude $\omega_{\text{eff}} \equiv \omega(a)$ and it is the interrelation between the detuning of the field with respect to the eigenfrequency and the damping $|\omega_F - \omega(a)|/\Gamma$ that determines the strength of the response. For small Γ, the latter ratio can vary markedly with a, even while $a \ll l_n$, and it is this feature that can give rise to the coexistence of different stable solutions for the amplitude a. We may

note that, for $a \ll l_n$, the vibrational amplitudes at the overtones are $\sim a^3/l_n^2 \ll a$, and dynamical chaotic phenomena do not occur. Because the noise intensities to be considered here are relatively weak, the system seldom strays far from the attractors and practically never goes as far as l_n; the probability of finding it there is exponentially small compared to the probabilities of transitions.

Under conditions for which $|\gamma|\langle q^2\rangle \ll \omega_F^2$, the motion of the oscillator consists of relatively fast oscillations with slowly varying amplitude and phase. The characteristic scale for these variations is determined by the friction coefficient Γ and the detuning $\delta\omega$ of the field frequency ω_F with respect to the oscillator eigenfrequency ω_0: the characteristic scale for the coordinate q is $|\gamma/\omega_F\delta\omega|^{-\frac{1}{2}}$. In describing the "slow" motion it is convenient, in the spirit of a standard averaging method (cf. [17]) to transform to the rotating frame. We thus change from $q, \dot{q}$ to the complex dimensionless envelopes u, u^* and the dimensionless time τ,

$$\begin{aligned} q &= \left(\frac{2\omega_F|\delta\omega|}{3|\gamma|}\right)^{\frac{1}{2}} \left(ue^{i\omega_F t} + u^* e^{-i\omega_F t}\right) , \\ \dot{q} &= i\omega_F \left(\frac{2\omega_F|\delta\omega|}{3|\gamma|}\right)^{\frac{1}{2}} \left(ue^{i\omega_F t} - u^* e^{-i\omega_F t}\right) , \\ \tau &= |\delta\omega| t . \end{aligned} \tag{5}$$

The equation of motion in terms of the variable u following from (3) – (5) takes the form

$$\frac{du}{d\tau} = v + \eta\tilde{f}(\tau) , \tag{6}$$

$$v \equiv v(u,u^*) = -\eta u + iu(|u|^2 - 1) - i\beta^{\frac{1}{2}} ,$$

where

$$\eta = \Gamma/\delta\omega, \qquad \beta = \frac{3\gamma F^2}{32\omega_F^3\delta\omega^3} \tag{7}$$

are, respectively, the reduced damping coefficient and the dimensionless field intensity. Equations (7) as written correspond to the particular case

$$\delta\omega > 0, \qquad \gamma > 0 . \tag{8}$$

The generalization to the case where the signs of $\delta\omega$ and γ are arbitrary is straightforward. We note that bistability can occur only for $\gamma\delta\omega > 0$; simultaneous change in the signs of γ and $\delta\omega$ will result in mirror reflection of the spectra considered below with respect to ω_F.

The random force $\tilde{f}(\tau)$ appearing in (6) is proportional to $f(t)$ in (3),

$$\tilde{f}(\tau) = -i\left(\frac{3\gamma}{8\omega_F^3\Gamma^2|\delta\omega|}\right)^{\frac{1}{2}} \exp(-i\omega_F t) f(t) \tag{9}$$

and, if $f(t)$ is Gaussian white noise of characteristic intensity B such that

$$\langle f(t)\, f(t')\rangle = 2\Gamma B\delta(t-t') , \tag{10}$$

then $\tilde{f}(\tau)$ is asymptotically a two-component white noise,

$$\begin{aligned} &\langle \tilde{f}(\tau)\, \tilde{f}(\tau')\rangle = \langle \tilde{f}^*(\tau)\tilde{f}^*(\tau')\rangle = 0 , \\ &\langle \tilde{f}(\tau)\tilde{f}^*(\tau')\rangle = 4\alpha\delta(\tau-\tau') , \\ &\alpha = \frac{3\gamma B}{16\omega_F^3\Gamma} . \end{aligned} \tag{11}$$

The correlator $\langle \mathrm{Re}\tilde{f}(\tau)\mathrm{Im}\tilde{f}(\tau')\rangle$ is fast oscillating; the slow variables u, u^* therefore perceive the components $\mathrm{Re}\tilde{f}(\tau)$,$\mathrm{Im}\tilde{f}(\tau)$ as independent white noises of equal intensity, which is why the correlators $\langle \tilde{f}(\tau)\tilde{f}(\tau')\rangle$ and $\langle \tilde{f}^*(\tau)\tilde{f}^*(\tau')\rangle$ are set equal to zero in (11). We also note that the relations (11) can be asymptotically fulfilled even where the initial noise $f(t)$ is not δ correlated; it suffices that its correlation time is small as compared with the "slow" process times $|\delta\omega|^{-1}, \Gamma^{-1}$ (but not necessarily as compared with ω_F^{-1} [3]).

The dynamics of the system (6) depends on the values of the three dimensionless parameters involved: η, β, and α. We shall assume the noise to be weak, so that

$$\alpha \ll 1 . \tag{12}$$

To zeroth order in $\tilde{f}(\tau)$, Eq. (6) describes the autonomous motion (note that we consider it in the frame rotating with the frequency of the external field) of a system with one degree of freedom and, correspondingly, with two dynamical variables u and u^* (or Reu and Imu). The stationary solutions of the equation $du/d\tau = v$ give, in accordance with (5), the states of steady forced vibration of the oscillator. The values of the complex envelope u in the steady states follow from the relation $v = 0$ and are given by

$$\begin{aligned} &u_j = \sqrt{\beta}(|u_j|^2 - 1 + i\eta)^{-1}, \quad \phi(|u_j|^2) = 0, \\ &\phi(x) = x(x-1)^2 + \eta^2 x - \beta , \end{aligned} \tag{13}$$

where j enumerates the real roots of the cubic equation (13) and can take on the value 1, 2, or 3. Equation (13) is readily interpreted. As a result of nonlinearity, the frequency of the eigenvibrations of the oscillator depends on their amplitude a as

$$\omega(a) \simeq \omega_0 + \frac{3}{8}\gamma a^2/\omega_0 .$$

On substitution of this expression into the well-known expression for the amplitude of the forced vibrations of a linear damped oscillator of frequency $\omega(a)$

$$a^2 = \frac{F^2}{[\omega_F^2 - \omega^2(a)]^2 + 4\omega_F^2\Gamma^2}$$

with account taken of the relation $a^2 = \frac{8}{3}|u|^2\omega_F|\delta\omega|/|\gamma|$, which follows immediately from (5), one simply obtains the cubic equation

$$\phi(|u|^2) = 0.$$

In the parameter range where this equation has three real roots, the oscillator is bistable: the forced vibrations with the smallest [$j = 1$ in (13)] and the largest ($j = 2$) ampli-

tudes are stable; there is also the unstable steady state $j = 3$ with an intermediate value of $|u_j|^2 \propto a_j^2$. The phase of the stable forced vibrations is determined by the argument of u_j in (13). The range of β, η for which (13) has three solutions, and thus bistability occurs, corresponds to the approximately triangular region bounded by the full curves $\beta_B^{(1,2)}(\eta)$ of Fig. 1, i.e., the bifurcation curves.

Thus, as the amplitude of the periodic force is gradually increased from a small value at fixed frequency (see, e.g., the vertical line $a - a'$ in Fig. 1), the system moves from monostability (one small limit cycle), to bistability (two possible limit cycles of different amplitude), and then back again to monostability (one large limit cycle). Some analogy can be drawn between the bistability and the liquid-gas coexistence region of a van der Waals system. As the spinode point, which corresponds to the van der Waals critical point, is approached, the two stable (and one unstable) solutions of (13), and, correspondingly, the amplitudes of the large and small limit cycles (liquid and gaseous phases) approach each other, to become indistinguishable at the spinode (critical point) itself. Consequently, just as in the van der Waals case, it is possible to move quasistatically from an initial state that is a small limit cycle (gaseous state) to a final state that is a large limit cycle (liquid state) without undergoing the analog of a first-order phase transition or passing through a mixed-phase coexistence region: all that is necessary is to take a route through the parameter space that passes outside the spinode (the critical point).

The above analysis makes sense provided that the basins of attraction are smooth and regular throughout the region of phase space likely to be visited by the system. The basins have been computed within the bistable regime (see Fig. 1) in the absence of noise and are shown as Poincaré sections (values of $\dot{q}, q$ for $t = 2\pi n\omega_F^{-1} + \phi_0$) in Fig. 2. We emphasize that the data in Fig. 2 refer to the initial oscillator described by (3) with $f(t) = 0$. In addition to the dimensionless parameters η, β, this system is characterized by the parameter Γ/ω_F which, in the present case, was set as $\Gamma/\omega_F = 0.0184$. The results were obtained by the usual "grid of starts" method [15], allowing the system to evolve from different starting points in the $(\dot{q}, q)$ phase space and noting in each case the attractor to which it was drawn. Thus all starts in white areas lead to the large amplitude attractor (the solid circle in the white area) and all starts in black areas lead to the small amplitude attractor (the solid circle in the black area). Figure 2 shows the evolution of the basins with increasing β for fixed η as Poincaré sections for the same phase. It is intuitively reasonable that the black basin (for the small amplitude attractor) should be dominant at small β, just within the region of bistability. As β increases, the white basin (for the large amplitude attractor) grows until the central regions of the two basins have become equal in area. With further increase of β the black basin continues to shrink, finally disappearing

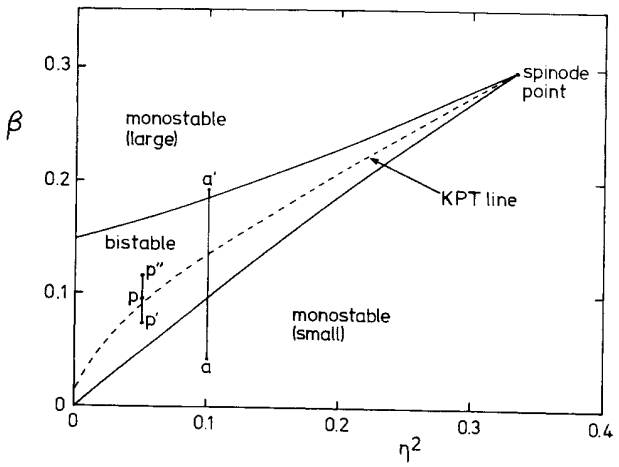

FIG. 1. Phase diagram for the system (3) in terms of the reduced parameters (7). Within the approximately triangular region enclosed by the full lines, the system is bistable, with two possible stable limit cycles of different amplitude and phase relative to the periodic driving force. Outside this region, the system is monostable. The dashed line represents the calculated position of the kinetic phase transition. The cuts a-a' and p'-p-p'' are discussed in the text.

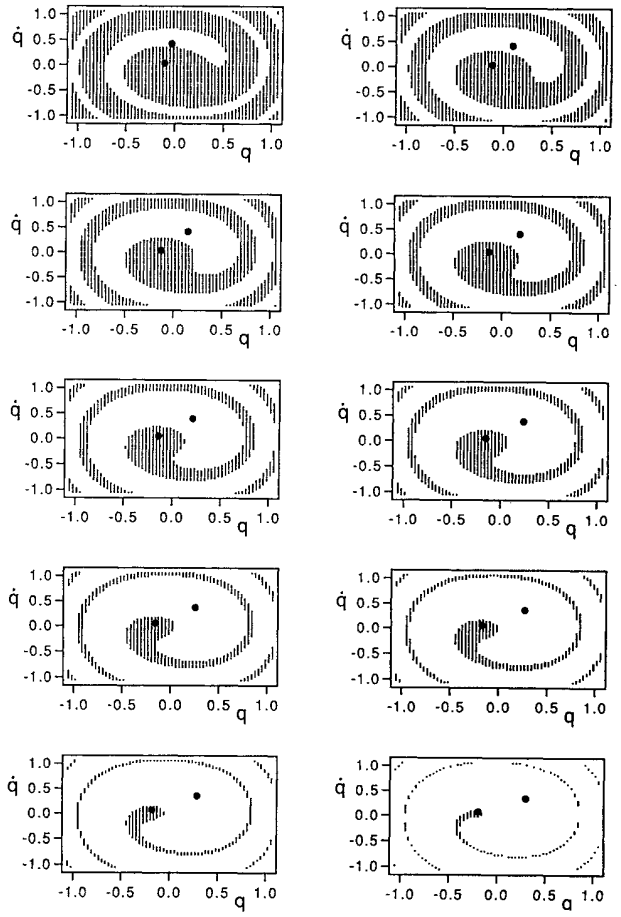

FIG. 2. The evolution of the basins of attraction for (3), computed for $\eta^2 = 0.072$ in Poincaré section with the same phase as that of the driving field. The white regions show the basin of attraction for the large amplitude attractor and the black regions show the basin for the small one; each attractor is indicated by a •. The values of β, first left-to-right, then top-to-bottom, were 0.0709, 0.0811, 0.0913, 0.102, 0.112, 0.122, 0.132, 0.143, 0.153, and 0.163.

at the upper boundary (Fig. 1) of the bistable region.

The most important feature of Fig. 2 for present purposes is that it confirms the basins to be (within the range and resolution of the computations) simple, smooth, and regular, as already stated above. The shapes and positions of the attractors are close to those given by the approximate equations of motion (6) in the absence of noise; we note that the latter equations do not display chaos or fractal boundaries. Because we are interested in the regime of weak noise intensity for which the system only makes *occasional* transitions between the attractors, we can be confident that it spends almost all of its time in the close vicinity of either one or other of them and that the probability of fluctuations carrying it out to regions of phase space where the basins might be irregular or fractal (far beyond the range plotted in Fig. 2) is exponentially small.

Finally in this section, we draw attention to the importance of a slightly different model, closely related to (3), that is likely to be more easily realized in experiments on systems excited by laser radiation with a randomly varying amplitude:

$$\ddot{q} + 2\Gamma\dot{q} + \omega_0^2 q + \gamma q^3 = [F + f(t)] \cos\omega_F t. \tag{14}$$

The significance of (14) arises because of the very high value of the driving frequencies ω_F in optical experiments, which means that external noise $f(t)$ introduced from a conventional noise generator will in practice be far from white; indeed the cutoff frequency of the generator is likely to be much *smaller* than ω_F.

Nevertheless, transforming (14) to the rotating frame again gives Eq. (6), except that the noise is now given by

$$\tilde{f}(\tau) = -\frac{i}{2}\left(\frac{3\gamma}{8\omega_F^3\Gamma^2|\delta\omega|}\right)^{\frac{1}{2}} f(t)$$

plus a term which varies as $f(t)\exp(2i\omega t)$. The limited spectral width of $f(t)$ that we have assumed implies that this term will only have a very small effect on the equation of motion of the slow variable $u(t)$. It is the high-frequency components of the noise that determine the random dynamics of a nearly-resonantly-driven underdamped nonlinear oscillator; the components of the noise with frequencies far from ω_0 are filtered out. In contrast to $\tilde{f}(\tau)$ (9), the new $\tilde{f}(\tau)$ has correlator

$$\langle\tilde{f}(\tau)\tilde{f}(\tau')\rangle = \langle\tilde{f}^*(\tau)\tilde{f}^*(\tau')\rangle = -\alpha\delta(\tau-\tau') ,$$
$$\langle\tilde{f}(\tau)\tilde{f}^*(\tau')\rangle = \alpha\delta(\tau-\tau') ,$$

i.e., instead of two independent components, the new $\tilde{f}(\tau)$ has only one. Nonetheless, the analysis presented below can be easily extended to give similar results for the system (14). Modulation of the periodic driving force by noise has pushed the effect of low-frequency noise into the high-frequency range.

B. Transition probabilities and the spectral density of fluctuations

The most obvious effects of noise on the behavior of the oscillator are, first, the onset of fluctuations about the stable states and, second, the occurrence of fluctuation-induced transitions between the states. Provided that the noise is weak, in accordance with (12), the system will spend most of its time in the close vicinity of one of the stable states: only very rarely will a sufficiently large fluctuation occur to cause a transition to the other stable state. The dependences of the probabilities W_{ij} of the transitions on the characteristic noise intensity are of the activation type:

$$W_{ij} = \text{const} \times \exp(-R_i/\alpha) . \tag{15}$$

The activation energy R_i for the transition from state i is given by the solution of a variational problem: the corresponding variational equations and the algorithm for their numerical solution are discussed in the Appendix. The resultant dependences of R_i on β for the lower ($i = 1$) and higher ($i = 2$) amplitudes of the forced vibrations in the limit of small reduced damping η were considered in [3]. Numerical results for four values of η are shown by the circles in Figs. 3(a)–3(d). It is evident that R_1 decreases and R_2 increases monotonically with increasing β, i.e., with the characteristic resonant field intensity. For the values of β corresponding to the upper and lower bifurcation lines $\beta_B^{(1,2)}$ in Fig. 1, R_1 and R_2 respectively vanish (as the states 1 and 2 coalesce with the saddle point and then disappear). The dependence of R_i on β for β close to $\beta_B^{(i)}(\Omega)$ is universal, $R_i = G_i(\eta)|\beta - \beta_B^{(i)}(\eta)|^{3/2}$, and is shown by the full lines. [The explicit form of G_i has been considered earlier; cf. [3(b)].] The numerical and asymptotic results are in good agreement for not too small η, where the optimal path of the escape [in the rotating frame (5): see the Appendix] is not a small-step spiral. For small η, however, the numerical algorithm is not accurate enough and results in the discrepancies seen in Fig. 3(a); as discussed in the Appendix, the data in this range can better be obtained in a different way. The dependence of $R_{1,2}$ on the frequency detuning η for β lying in the central part of the interval $[\beta_B^{(1)}(\eta), \beta_B^{(2)}(\eta)]$ is rather sharp, especially at small η where [3] $R_{1,2} \propto \eta^{-1}$. As η approaches its critical value (the spinode point in Fig. 1) given by

$$\eta_K^{-1} = \sqrt{3}, \qquad \beta_K = 8/27,$$

the values of $R_{1,2}$ decrease rapidly [3], as $(\eta-\eta_K)^2$. Here too the numerical and analytic results are in good agreement. It is evident that, as η approaches η_K, the range of β over which R_i is well described by the asymptotic law $|\beta - \beta_B^{(i)}(\eta)|^{3/2}$ increases relative to the total range of bistability $|\beta_B^{(2)}(\eta) - \beta_B^{(1)}(\eta)|$. Qualitatively, this is related to the fact that the optimal path of the escape is approaching a straight line on the (Reu,Imu) and it becomes nearly straight for all β, η close to the spinode point.

The analytic and calculated values of R_1 and R_2 allow us to plot on Fig. 1 the dashed curve $\beta_0(\eta)$ specifying the points at which the activation energies are equal, closely approximating the line of the kinetic phase transition (KPT) at which the populations are equal,

$$R_1(\beta,\eta) = R_2(\beta,\eta), \quad \beta = \beta_0(\eta). \tag{16}$$

[Note that the criterion $R_1 = R_2$ differs from $w_1 = w_2$ only by virtue of variations in the prefactor $\sim \alpha$ in (15); the criteria become identical as $\alpha \to 0$.] For parameter values far from this curve, the transition probabilities W_{12} and W_{21} are seen from (15) to differ exponentially strongly. Correspondingly, the stationary populations w_1, w_2 of the states as given by (2) are also exponentially different,

$$w_1/w_2 \propto \exp[(R_1 - R_2)/\alpha] .$$

Only in the close vicinity of the $\beta_0(\eta)$ curve will the transition probabilities and stationary populations be comparable and it is here, therefore, that one may expect to observe the characteristic steady-state fluctuation phenomena associated with transitions between the attractors; we do not consider here the transient fluctuation effects that arise when, for example, the parameters are swept through the bifurcation lines in Fig. 1.

A revealing characteristic property of a fluctuating system is its spectral density of fluctuations. The SDF of the coordinate of a periodically driven oscillator $Q(\omega)$ is given by

$$Q(\omega) = \frac{1}{\pi} \mathrm{Re} \int_0^\infty dt \exp(i\omega t)\tilde{Q}(t) ,$$

$$\tilde{Q}(t) = \lim_{T\to\infty} \frac{1}{2T} \int_{-T}^{T} d\tau \, [q(t+\tau) - \langle q(t+\tau)\rangle] \times [q(\tau) - \langle q(\tau)\rangle] . \tag{17}$$

We note that a periodically driven system is in general nonergodic, so that $\tilde{Q}(t)$ is not equal to the time correlation function

$$\langle [q(t+\tau) - \langle q(t+\tau)\rangle][q(\tau) - \langle q(\tau)\rangle]\rangle ,$$

defined in terms of ensemble averaging $\langle\,\rangle$; in fact, the latter quantity oscillates with τ at frequency ω_F, as can be seen from (5) and (6); $\tilde{Q}(t)$ actually corresponds to this quantity smoothed over τ.

The ensemble-averaged value of the coordinate $\langle q(t)\rangle$ is equal to the value of $q(t)$ averaged over equal instants of time modulo $2\pi/\omega_F$,

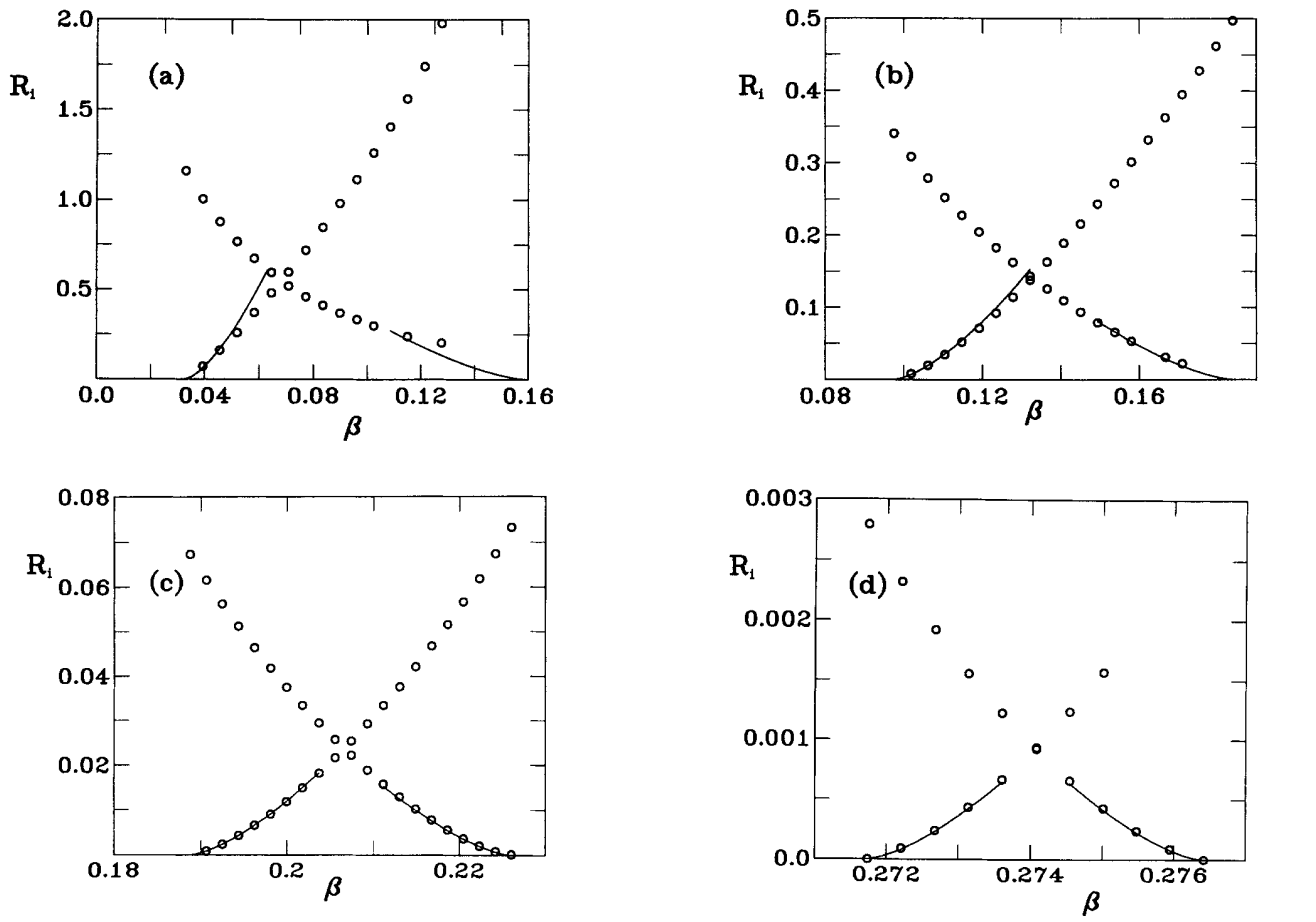

FIG. 3. Calculated activation energies R_i for transitions between the coexisting periodic attractors of (3), as functions of β for (a) $\eta^2 = 0.033$, (b) $\eta^2 = 0.100$, (c) $\eta^2 = 0.200$, and (d) $\eta^2 = 0.333$. The circle data points were obtained by minimization of the action integral R_j in Eq. (A1); the curves are derived from analytic expansions [3(b)] around the relevant bifurcation points. In each case, the falling data and curve represent R_1 and the rising data and curve represent R_2.

$$\langle q(t)\rangle = \lim_{N\to\infty} N^{-1}\sum_{n=0}^{N-1} q(t+2\pi n\omega_F^{-1}).$$

In the case of weak noise, two principal contributions to $Q(\omega)$ can be identified [12,18]. The first of these arises from small fluctuations about the stable states. It is equal to the sum over the states j of the corresponding partial SDFs, $Q_j(\omega)$, weighted by the state populations w_j given by (2) (cf. also [19]). The second contribution $Q_{\rm tr}(\omega)$ comes from the (relatively infrequent) fluctuational transitions between the states. Thus (cf. [5])

$$Q(\omega) = \sum_j w_j Q_j(\omega) + Q_{\rm tr}(\omega)\,. \tag{18}$$

To calculate the partial SDF, $Q_j(\omega)$, for the state j when the noise intensity α is small, it suffices to linearize the v term on the right hand side of (6) with respect to small deviations in $(u-u_j),(u^*-u_j^*)$, to substitute the solution of the resultant linear equations into (17), taking due account of (5), and to perform averaging. The result is of the form

$$Q_j(\omega) = \frac{4\omega_F\alpha\Gamma^2}{3|\gamma|\pi}\,\frac{(\omega-\omega_F)^2+2(\omega-\omega_F)\Gamma\eta^{-1}(2|u_j|^2-1)+\Gamma^2(\nu_j^2+2\eta^{-2}|u_j|^4)}{[(\omega-\omega_F)^2-\Gamma^2\nu_j^2]^2+4\Gamma^2(\omega-\omega_F)^2}\,,$$

$$\nu_j^2 = 1+\eta^{-2}(3|u_j|^2-1)(|u_j|^2-1)\,, \tag{19}$$

where $|u_j|^2$ for $j=1,2$ is given by Eq. (13). It is evident from (19) that $Q_j(\omega)$ is peaked near the frequency ω_F of the external field. Its intensity will be proportional to the noise intensity. The shape of $Q_j(\omega)$ will be discussed in Sec. IV.

The second term in (18), $Q_{\rm tr}(\omega)$, can readily be calculated if one notes that the populations w_j of the stable states fluctuate in time with a characteristic relaxation time $(W_{12}+W_{21})^{-1}$, so that

$$\frac{dw_1(t)}{dt} = -(W_{12}+W_{21})w_1(t)+W_{21}\,,$$
$$w_2(t) = 1-w_1(t)\,. \tag{20}$$

[The values of w_j appearing in (2) and (18) correspond to the stationary solutions of (20).] In the case of weak noise, these fluctuations can be shown [12] to result in a contribution to $Q(\omega)$ of

$$Q_{\rm tr}(\omega) = \frac{2\omega_F|\omega_F-\omega_0|}{3\pi|\gamma|}|\langle u_1\rangle-\langle u_2\rangle|^2 w_1w_2 \times\frac{W_{12}+W_{21}}{(W_{12}+W_{21})^2+(\omega-\omega_F)^2}\,. \tag{21}$$

Here $\langle u\rangle_j$ denotes the ensemble average value of u in the state j. In the zero noise limit $\langle u\rangle_j$ is simply u_j. For the purposes of comparison with experiments performed at finite noise intensity, $\langle u\rangle_j$ can be expanded as a perturbation series in the small parameter α. To first order we obtain

$$\langle u\rangle_j = u_j+\langle\delta u_j\rangle\,,$$

$$\langle\delta u_j\rangle = \frac{2\alpha u_j}{\eta^3\nu_j^4}\{\,i\eta[2\eta^2+3|u_j|^4-6|u_j|^2+2] -(3|u_j|^2-2)(\eta^2+2|u_j|^4-3|u_j|^2+1)\}\,.$$

We note that the spectral peak $Q_{\rm tr}(\omega)$ is extremely narrow: its width is determined by the transition probabilities, so that it is exponentially small and much smaller than the damping parameter Γ which determines the "dynamical" relaxation of the oscillator towards either of its stable states. The product w_1w_2, which determines the intensity of $Q_{\rm tr}(\omega)$, can be seen from (2) and (15) to be exponentially small for almost all values of β,η, with the exception of those within the very narrow range (the phase-transition region) where $w_1\sim w_2\sim 1$. Thus the onset of the fluctuational transition-induced spectral peak $Q_{\rm tr}(\omega)$ is a specific phase-transition phenomenon (see Sec. IV).

C. The susceptibility and the high-frequency stochastic resonance

The effect of a weak trial periodic force on thermal equilibrium systems is the onset of vibrations at the frequency of the force; their amplitude is characterized by a susceptibility, which can be expressed in terms of the SDF via the fluctuation dissipation theorem [20]. If the system is being driven by a strong periodic force $F\cos\omega_F t$, so that it is far from thermal equilibrium, the additional weak force $A\exp(-i\Omega t)$ gives rise to vibrations not only at its own frequency Ω, but also at combination frequencies $|\Omega\pm\omega_F|, |\Omega\pm 2\omega_F|, \ldots$.

We shall consider the linear response of the bistable oscillator to a nearly resonant trial force with a frequency Ω close to ω_0,ω_F:

$$|\Omega-\omega_0|,\quad |\Omega-\omega_F| \ll \omega_F\,.$$

In this case, a strong response is to be expected. It will be most pronounced at the frequency Ω and at the nearest resonant combination frequency, which is $2\omega_F-\Omega$. Thus one can seek the trial force-induced modification of the ensemble-averaged coordinate q in the form

$$\delta\langle q(t)\rangle \simeq \chi(\Omega)A\exp(-i\Omega t) + X(\Omega)A\exp[i(2\omega_F-\Omega)t]\,. \tag{22}$$

That is, we may suppose that the linear response is characterized by two coefficients (generalized susceptibilities)

$\chi(\Omega)$ and $X(\Omega)$. The absorption (amplification) of the trial field is characterized by $\mathrm{Im}\chi(\Omega)$. It was shown in [3] that, in the vicinity of the KPT, interesting features occur in the absorption spectrum.

To calculate the susceptibilities we transform to the slow variables u, u^* (5) in the equation of motion (3) with the additional force $A\exp(-i\Omega t)$ added to the right hand side. The resultant equations for u, u^* take the form

$$\frac{du}{d\tau} = v(u,u^*) + \eta\tilde{f}(\tau)\,,$$

$$\frac{du^*}{d\tau} = v^*(u,u^*) + \eta\tilde{f}^*(\tau) + i\tilde{A}(\tau)\,, \qquad (23)$$

$$\tilde{A}(\tau) = \left[\frac{3|\gamma|}{8\omega_F^3|\delta\omega|^3}\right]^{\frac{1}{2}} A\exp\left[\frac{-i(\Omega-\omega_F)\tau}{|\delta\omega|}\right].$$

It is evident from (23) how the second term in (22) arises: it is due to the addition $\propto \exp[-i(\Omega-\omega_F)t]$ to u, which is then multiplied by $\exp(i\omega_F t)$ when $q(t)$ is calculated in (5).

If the random force $\tilde{f}(\tau)$ is weak, the main effects of the additional term $\propto \tilde{A}(\tau)$ in (23) are (i) to cause small amplitude periodic vibrations of u, u^* about their stable values u_j, u_j^* and (ii) via the change in the probabilities of fluctuational transitions to modulate periodically the populations of the stable states. These effects give rise to expressions for the generalized susceptibilities of the form

$$\chi(\Omega) = \sum_j w_j\chi_j(\Omega) + \chi_{\mathrm{tr}}(\Omega)\,,$$

$$X(\Omega) = \sum_j w_j X_j(\Omega) + X_{\mathrm{tr}}(\Omega)\,, \qquad (24)$$

where χ_j, X_j are the partial susceptibilities related to the corresponding vibrations about the stable states and $\chi_{\mathrm{tr}}, X_{\mathrm{tr}}$ are related to the trial force-induced redistribution over the states.

The partial susceptibilities can readily be calculated by linearizing (23) near the stable states, yielding

$$\chi_j(\Omega) = \frac{i}{2\omega_F}\,\frac{\Gamma - i(\Omega-\omega_F) - i(2|u_j|^2-1)(\omega_F-\omega_0)}{\Gamma^2\nu_j^2 - 2i\Gamma(\Omega-\omega_F) - (\Omega-\omega_F)^2}\,,$$

$$X_j(\Omega) = \frac{-1}{2\omega_F}\,\frac{u_j^2(\omega_F-\omega_0)}{\Gamma^2\nu_j^2 - 2i\Gamma(\Omega-\omega_F) - (\Omega-\omega_F)^2}\,. \qquad (25)$$

The effective modulation of the transition probabilities by the trial field A, which gives rise to the second term on the right hand side of each of Eq. (24), arises when its frequency Ω is very close to ω_F, so that

$$|\Omega-\omega_F| \ll \Gamma,\ |\omega_F-\omega_0|\,.$$

In this case, the trial field smoothly raises and lowers the effective "barrier" between the stable states with the period $2\pi/|\Omega-\omega_F|$, so that the activation energies R_1, R_2 of the fluctuational transitions vary periodically in time [3]. The corresponding additions to R_j are given in the Appendix. In turn, they give rise to periodic additions to the transition probabilities W_{ij} (15) and hence to the populations w_j of the stable states (20). The final expression for the redistribution-induced additions to the generalized susceptibilities is

$$\chi_{\mathrm{tr}}(\Omega) = \frac{w_1w_2}{2\omega_F(\omega_F-\omega_0)}(\langle u\rangle_1^* - \langle u\rangle_2^*)\left(\frac{\mu_1-\mu_2}{\alpha}\right) \times\left[1-\frac{i(\Omega-\omega_F)}{W_{12}+W_{21}}\right]^{-1},$$

$$X_{\mathrm{tr}}(\Omega) = \frac{\langle u\rangle_1 - \langle u\rangle_2}{\langle u\rangle_1^* - \langle u\rangle_2^*}\,\chi_{\mathrm{tr}}(\Omega)\,, \qquad (26)$$

$$\mu_j = \sqrt{\beta}\left(\frac{\partial R_j}{\partial\beta}\right).$$

It is evident from (26) that the susceptibilities $\chi_{\mathrm{tr}}(\Omega), X_{\mathrm{tr}}(\Omega)$ are large only within the range of parameters β, η, close to the kinetic phase transition, where the populations w_1, w_2 of the stable states are of the same order of magnitude. The characteristic range of the frequency Ω of the trial field within which these susceptibilities are large is determined by the transition probabilities. Consequently, it increases exponentially with increasing noise intensity (cf. [12]). This property gives rise to *stochastic resonance* [8], i.e., to an increase of the signal-to-noise ratio (SNR) with increasing noise [21] which, as shown below, occurs in the present system for a high-frequency signal $\Omega \simeq \omega_F \gg \Gamma$. To calculate the SNR, we note from (22) that the signal induced by a real field $A\cos\Omega t$ is given by

$$\delta\langle q(t)\rangle = A\,\mathrm{Re}\Big\{\chi(\Omega)\exp(-i\Omega t) + X(\Omega)\exp[i(2\omega_F-\Omega)t]\Big\}. \qquad (27)$$

Such a signal corresponds to the appearance of δ-shaped spikes in the power spectrum of the oscillator at frequencies Ω and $(2\omega_F-\Omega)$. This can be seen from (17) if (27) is added to $q(t), q(t+\tau)$ but not to $\langle q(t)\rangle$. [The latter quantity is included in (17) to subtract the δ function in $Q(\omega)$ at the frequency ω_F of the strong field.] It is evident from (16) and (17) that the ratios P and $\mathcal{P}$ of the strengths (areas) of the spikes at frequency Ω of the trial field, and at the combined frequency $(2\omega_F-\Omega)$, to the power spectrum in the absence of noise are given by

$$P = \frac{\mathcal{S}}{\mathcal{Q}(\otimes)}, \qquad \mathcal{P} = \frac{\mathcal{S}}{\mathcal{Q}(\in\omega_{\mathcal{F}}-\otimes)}\,, \qquad (28)$$

$$S = \frac{1}{4}A^2|\chi(\Omega)|^2, \qquad \mathcal{S} = \frac{1}{4}A^2|X(\Omega)|^2\,.$$

It follows from (25) that the "partial" susceptibilities $\chi_j(\Omega), X_j(\Omega)$ are independent of noise for weak noise,

whereas the partial contributions to the SDF $Q_j(\Omega)$ increase linearly with the noise intensity. Far from the phase-transition region, therefore, where the fluctuational transition contributions to the susceptibilities and SDF are small, the quantities P and $\mathcal{P}$ decrease with increasing noise. Within the phase-transition range, on the other hand, for small $|\Omega-\omega_F| \sim W_{ij}$, the main contribution to $\chi(\Omega)$, $X(\Omega)$, and $Q(\Omega)$ comes from the transitions (26) and (21). This is because their ratio to the corresponding partial contributions is inversely proportional to $\alpha \ll 1$, in the case of $\chi(\Omega)$, $X(\Omega)$, and to $W_{ij}/\Gamma \ll 1$, in the case of $Q(\Omega)$. If only $\chi_{\rm tr}$, $X_{\rm tr}$, and $Q_{\rm tr}$ are taken into account in (28), one obtains the corresponding quantities $P_{\rm tr}$, $\mathcal{P}_{\rm tr}$

$$P_{\rm tr} = \mathcal{P}_{\rm tr} = A^2 \frac{3\pi|\gamma|}{32\omega_F^3|\omega_F-\omega_0|^3}\left(\frac{\mu_1-\mu_2}{\alpha}\right)^2 \times \frac{W_{12}W_{21}}{W_{12}+W_{21}} . \tag{29}$$

According to (29), the quantities $P_{\rm tr}, \mathcal{P}_{\rm tr}$ are independent of frequency. At the same time, they can be seen from (15) to increase exponentially with increasing noise intensity. This implies the onset of high-frequency stochastic resonance within the phase-transition range, not only at the frequency of the trial field, but also at the combination frequency $(2\omega_F-\Omega)$. In fact, the ratio $\mathcal{P}$ is rather different from the quantity usually considered in the context of stochastic resonance, because no force is being applied at the frequency $|\Omega-2\omega_F|$: the signal is induced by mixing, in a nonlinear system, of the forces at frequencies Ω and ω_F. In relation to nonlinear optics [22], the phenomenon can be regarded as a type of highly selective, resonant, four-wave mixing (actually, multiwave mixing because the effect is not just proportional to the squared amplitude F of the strong field).

We would emphasize that stochastic resonance occurs only within the phase-transition region. When the parameters β, η of the oscillator are far from this region, the contributions $\chi_{\rm tr}, X_{\rm tr}, Q_{\rm tr}$ to the susceptibilities and the SDF in the absence of the trial force are exponentially small: P and $\mathcal{P}$ differ markedly from $P_{\rm tr}$ and $\mathcal{P}_{\rm tr}$, therefore, and decrease with increasing α. The dependences of P and $\mathcal{P}$ on α, as given by (18), (19), (21), (24)–(26), and (28), will be compared with the results of the analog electronic experiments in Sec. IV below.

III. ANALOG ELECTRONIC EXPERIMENTS ON THE PERIODICALLY DRIVEN OSCILLATOR

In order to test the theoretical predictions of the preceding section, and to find out whether they were applicable to a real physical system described by the model equation (3), a series of analog electronic experiments was undertaken. The basis of the analog technique has been described in detail elsewhere [23], together with a discussion of its advantages and disadvantages. In essence, it is extremely simple. An electronic model of the stochastic differential equation under study is built using standard analog components (operational amplifiers, multipliers, etc.). This is then driven by stochastic and periodic forces, as appropriate, and its response is analyzed with the aid of a digital data processor.

The circuit used to model (3) is shown in (slightly simplified) block form in Fig. 4; note that each analog multiplier yields an output equal to one-tenth of the product of the inputs and that the output can optionally be multiplied by -1 [23]. The circuit was designed and scaled in the standard [23] way so as to optimize use of the dynamic range of the active components. Thus the actual equation simulated (see Fig. 4) was the integral form of

$$R_1C_1R_4C_2\ddot{q} + \frac{R_1}{R_3}R_4C_2\dot{q} = -\frac{R_1}{R_5}q - \frac{R_1}{R_6}\frac{q^3}{20} + \frac{R_1}{R_2}F'\sin\omega_F' t + \frac{R_1}{R_0}A'\sin\Omega' t + f(t)$$

with

$$R_1 = R_4 = R_5 = 2R_6 = \frac{R_2}{10} = \frac{R_0}{10} = 100k\Omega ,$$

$$R_3 = 2.5M\Omega ,$$

$$C_1 = C_2 = 1nF ,$$

$$\tau = R_1C_1 = R_4C_2 ,$$

$$2\Gamma = R_1/R_3 .$$

Thus the equation actually simulated was

$$\tau^2\ddot{x} + 2\Gamma\tau\dot{x} = -x - \frac{x^3}{10} + \frac{F'}{10}\sin\omega_F' t + \frac{A}{10}\sin\Omega' t + f(t) ,$$

which, after the scaling

$$t \to t'/\tau, \quad \omega_F \to \omega_F'\tau, \quad \Omega \to \Omega'\tau, \quad F \to F'/10, \quad A \to A'/10 ,$$

goes over into (3) with $\omega_0 = 1$ and $\gamma = 0.1$. Provision was made for measuring either the coordinate $q(t)$ or the energy $E = \frac{1}{2}\dot{q}^2 + \frac{1}{2}q^2 + \frac{1}{4}\gamma q^4$.

The circuit model was driven with a sinusoidal periodic force from a Hewlett-Packard 3325B frequency synthesizer. Its response, a time-varying voltage representing $q(t)$, was digitized (12-bit precision) typically in $1k$ or $2k$ blocks and analyzed using a Nicolet Model LAB80 data processor; for the experiments on high-frequency stochas-

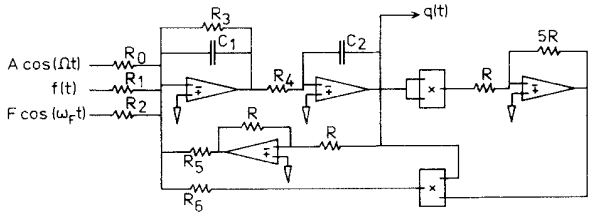

FIG. 4. Block diagram of the analog electronic circuit model of Eq. (3).

tic resonance, where larger $q(t)$ data blocks were required (see below), a Nicolet 1280 data processor was used.

As expected, the model was found to display bistability within a certain range of forcing amplitude and frequency: its response $q(t)$ in the absence of noise for a given set of parameters, shown in Fig. 5(a), could have either of two distinct amplitudes, corresponding to the two coexisting periodic attractors discussed in Sec. II. An inherent experimental difficulty of the measurements lay in the accurate determination of β, on account of the $|\omega_F - \omega_0|^3$ term in the denominator. Because, for the region of interest, the forcing frequency ω_F is very close to the natural (zero amplitude) frequency ω_0 of the oscillator, a very small error (typically $\pm$ 1%) in ω_0 inevitably results in a much larger error (typically $\pm$ 40%) in the value of β. For this reason, rather than attempting to determine ω_0 from the nominal component values or, directly, by a resonance experiment, its value was established precisely by measurement of the range of bistability at a single value of η. Once this had been done, the rest of the region of bistability could be mapped out over the whole range of η, resulting in the square data points of Fig. 6. They are seen to be in satisfactory agreement with the theoretical prediction of Sec. II (full curves).

The energy $E = \frac{1}{2}\dot{q}^2 + \frac{1}{2}q^2 + \frac{1}{4}\gamma q^4$ of the oscillator (apart from the coupling energy to the force), measured as a function of q in the absence of noise for each of the attractors, is shown in Fig. 5(b); it is of relevance because it provides a basis for the measurement of first-passage times between the stable states (see Sec. IV B). Both E and q are periodic functions of time, so that the energy can in principle take on several values for any given q, depending on how many times $\dot{q}$ becomes zero during one period $2\pi/\omega_F$. For the Duffing oscillator in the range of parameters considered here, where the nonlinearity is relatively small (see Sec. II A), $\dot{q}$ was zero twice within a period and therefore E could take on not more than two values for a given q. Since, for small enough nonlinearity, the steady vibrations $q(t)$ have components at the odd overtones only, i.e., at the frequencies $\omega_F, 3\omega_F, 5\omega_F, \ldots$, there is an additional symmetry: $q(t + \pi/\omega_F) = -q(t)$, $E(t+\pi/\omega_F) = E(t)$. Consequently, the energy is a unique function of the coordinate q on an attractor. We emphasize, however, that E is not conserved: the oscillator acquires energy from the periodic driving force and dissipates it through friction. It is evident from Fig. 5(b) that the curvature of $E(q)$ is relatively small, providing a clear indication that the amplitudes of the harmonics of $E(t)$ are also small; in the approximation (6), they have been ignored. The smearing (thickness) of the $E(q)$ lines in Fig. 5(b) is an experimental artifact: the values of E and q were recorded at discrete intervals of time, and neighboring pairs of values have been connected by straight lines [cf. Fig. 7(b)].

When noise was applied to the driven oscillator, fluctuations about the attractors and occasional transitions between them were observed. Figure 7(a) shows an experi-

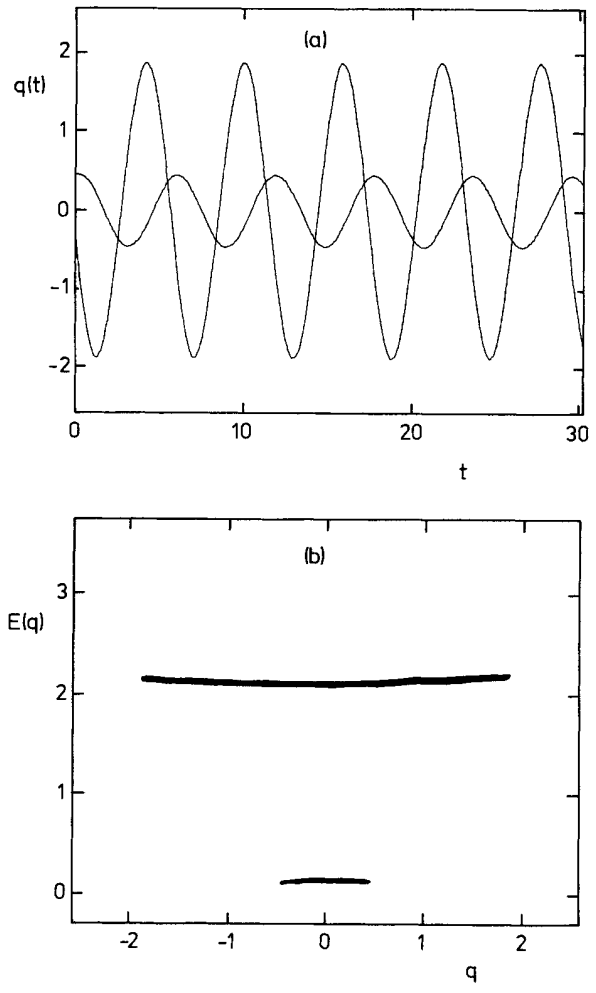

FIG. 5. (a) Variations of the coordinate $q(t)$ with time t, measured for the electronic circuit model of (3) within the bistable regime in the absence of noise with $\beta = 0.0607$ and $\eta^2 = 0.033$. Digitized time series for the small and large amplitude attractors are shown superimposed; note the phase difference between them. In (b) the instantaneous energy E of the system is plotted as a function of q: the lower curve is for the small amplitude attractor and the upper curve is for the larger one.

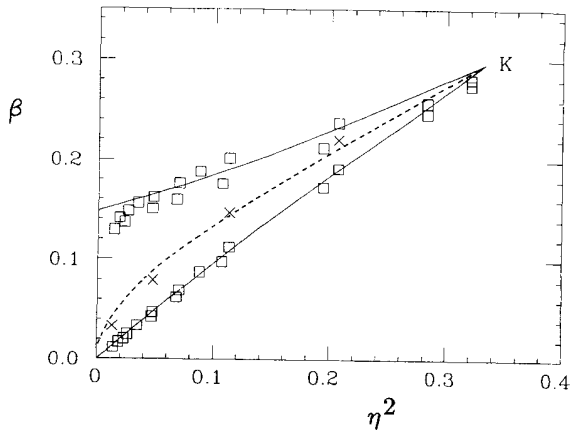

FIG. 6. Comparisons of the calculated region of bistability (between the full curves; cf. Fig. 1) with that measured for the electronic circuit model of (3) (square data points), and between the calculated (dashed line) and measured (crosses) kinetic phase transition line.

mental example of one such transition; the corresponding $E(q)$ plot in Fig. 7(b) shows the fluctuations in energy about each of the attractors, yielding an envelope that illustrates very clearly the shape of the potential [cf. Fig. 5(b) for the noise-free energies].

Measurement of the transition probabilities between the attractors was not completely straightforward because there was a small region of overlap between them in terms of any single variable whether measured, for example, in terms of $q(t)$ or of $E(q)$. Thus the determination of sojourn times [24] on either side of a fixed value of q or E would not have provided the information sought. Instead, the mean first-passage time (MFPT) was measured between *two* preset criterion levels in energy, which were outside the overlap region and unambiguously within each of the attractors. Figure 8(a) illustrates how the apparent MFPT varied when one criterion level was kept fixed within the lower energy attractor, and the other level was moved through different values. There is clearly a plateau region around the noise-free energy level of the attractor for which the MFPT was independent of level setting: all of the MFPT measurements to be reported below refer to this region.

To determine SDFs, a standard fast Fourier transform (FFT) routine was used to compute the power spectral density of the fluctuations $q(t) - \langle q(t)\rangle$. In practice, the ensemble-averaged signal $\langle q(t)\rangle$ was determined in a preliminary experiment for each set of parameters, averaging a large number (typically 1000) of blocks of $q(t)$ in order to obtain good statistical quality. This was possible because of $\langle q(t)\rangle$ being strictly periodic, with $\langle q(t)\rangle = \langle q(t + 2\pi/\omega_F)\rangle$, and because the phase of $\langle q(t)\rangle$ was determined with respect to that of the field $F\cos\omega_F t$. The resultant $\langle q(t)\rangle$ was then subtracted from

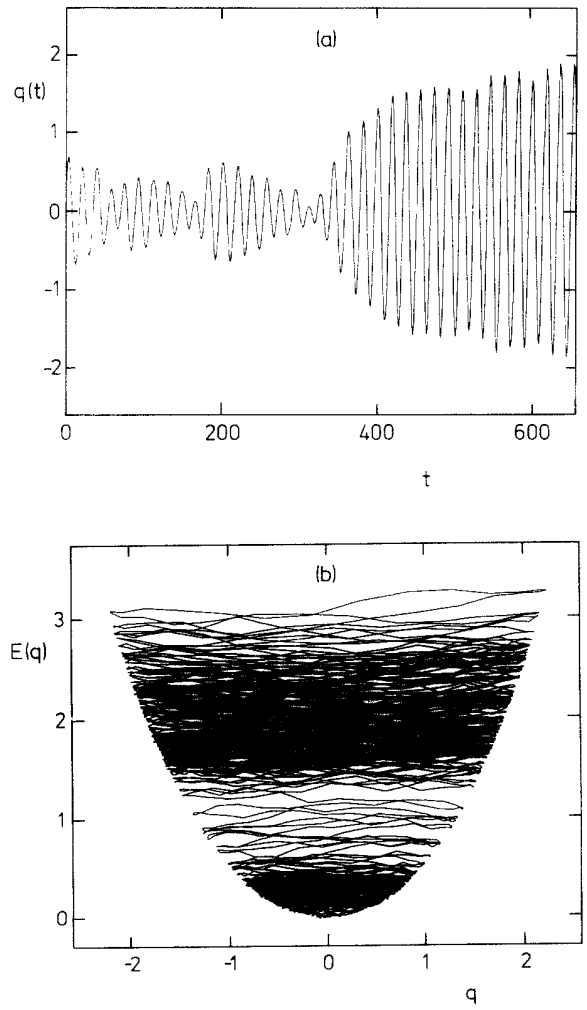

FIG. 7. (a) Variation of the coordinate $q(t)$ with time t, measured for the electronic circuit model of (3) in the bistable regime of the presence of noise with $\beta = 0.0607$ and $\eta^2 = 0.033$, showing a transition between the attractors (a rare event). (b) The corresponding variation of the instantaneous energy E with the coordinate q (cf. Fig. 5 in the absence of noise).

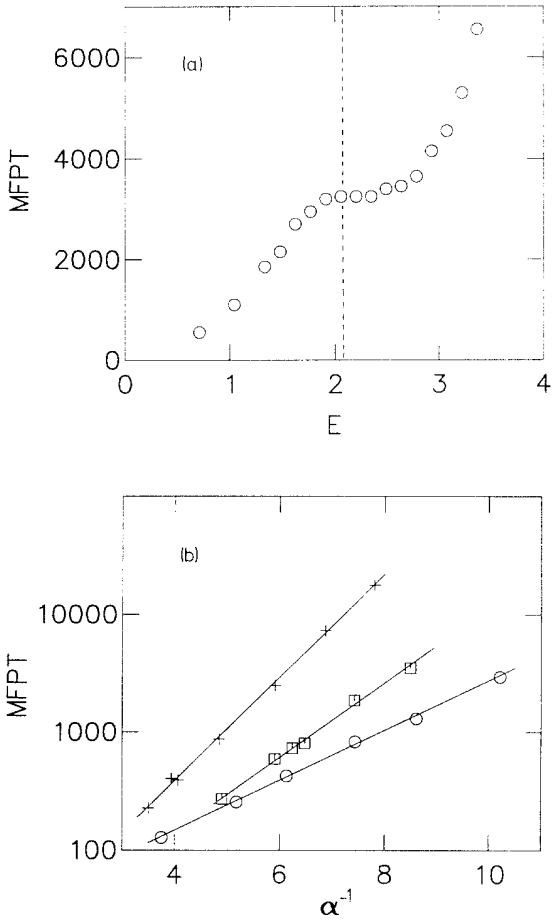

FIG. 8. (a) Dependence of the apparent mean first passage time on the position chosen for the upper criterion level for crossings: the energy of the larger attractor for $q = 0$ in the absence of noise is shown by the dashed line. In practice, all measurements were made in the plateau region. (b) Logarithmic plots of the MFPT between the attractors measured for the analog electronic circuit model of (3) as a function of reciprocal noise intensity α^{-1}, for $\eta^2 = 0.033$: +, from the small amplitude attractor with $\beta = 0.0888$; □, from the large attractor with $\beta = 0.047$; and ○, from the small attractor with $\beta = 0.0734$. The fact that the data lie on straight lines demonstrates the "thermal activation" character of the transition mechanism.

each subsequent realization of $q(t)$ before the FFT was applied to find the SDF, which was itself ensemble averaged to produce the final result.

The experiments on high-frequency stochastic resonance involved the application of an additional weak trial force $A\cos(\Omega t)$ to the system, with Ω very close to the main forcing frequency ω_F. In order to resolve the expected (see above) responses at Ω and at $|2\omega_F - \Omega|$ from the supernarrow peak at ω_F, it was necessary to use a relatively large block size, which in practice was set to $8k$ or $16k$ using the Nicolet 1280 data processor.

IV. DISCUSSION OF RESULTS

We now compare the theoretical predictions of Sec. II with the results of the analog experiments described in Sec. III. As already noted above, all of the main features expected on the basis of the theory have been observed in the simulations: for example, the anticipated bistability of the oscillator was observed and its range in terms of β, η was found (see comparison of data points and theory in Fig. 6) to be in agreement with the theoretical predictions; and with weak noise applied to the system, fluctuational transitions were observed to be taking place between the stable states. We now present a more detailed comparison of experiment and theory considering, in turn, escape probabilities, spectral densities of the fluctuations, and high-frequency stochastic resonance in Secs. IV A, IV B, and IV C, respectively.

A. Transition probabilities

To characterize the transition probabilities, the average lifetimes $\langle T_i \rangle$ of the states were measured (with the mean time $\langle T_i \rangle$ from the initially occupied state i being measured in the absence of backflow as described in Sec. III, so that

$$\langle T_i \rangle = W_{ij}^{-1} = -\int_0^\infty t(dw_i/dt)_0 dt$$

with $(dw_i/dt)_0 = -W_{ij}w_i$ and $w_i(0) = 1$). Some typical measurements of the average lifetime $\langle T_i \rangle = W_{ij}^{-1}$, on a log plot as a function of noise intensity α, are shown in Fig. 8(b). The fact that the data fall on straight lines confirms that the escape process is of the activation type, as expected on the basis of Eq. (15); the characteristic activation energies R_i of the transitions for given β, η can be obtained immediately from the slope in each case. Some experimental values of R_i, obtained in this way from a large number of measurements similar to those of Fig. 8, are presented in Fig. 9. In good qualitative agreement with the theoretical predictions (full curves), the value of R_1 for the transition from the lower amplitude attractor decreases monotonically with increasing dimensionless field intensity β, while R_2 for the transition from the higher amplitude attractor correspondingly increases. Both R_1 and R_2 increase with the increase of the frequency detuning parameter η^{-1}. Note that the experimental errors here are relatively large, due to the problem of measuring η, discussed above, and to the effect of small changes $\sim \pm 0.5\%$ in ω_0 with ambient temperature.

The values of β, η for which $R_1 = R_2$ lie extremely close to those values for which $\langle T_1 \rangle = \langle T_2 \rangle$ [because the effect of the prefactor in Eq. (15) is relatively weak], defining the kinetic phase transition. The phase-transition points obtained from the experimental data (for $\langle T_1 \rangle = \langle T_2 \rangle$, crosses) fall close to the position of the theoretical phase-transition line (for $R_1 = R_2$, dashed) in Fig. 6. The discrepancy between experiment and theory becomes somewhat larger near the spinode point K where the system is very "soft" and extremely weak noise intensities are necessary to make the transition region sufficiently narrow and the phase transition itself sufficiently sharp. The influence of uncertainties in the experimental parameters, and of internal noise in the active circuit components, becomes even more important here. Taking due account of all these factors, it may be concluded that theory and experiment are in satisfactory agreement.

B. Spectral density of fluctuations

Experimental measurements of the SDF in the vicinity of the oscillator eigenfrequency (histograms) are presented and compared with theory (full curves) in Figs. 10(a)–10(c). It must be emphasized that the measure-

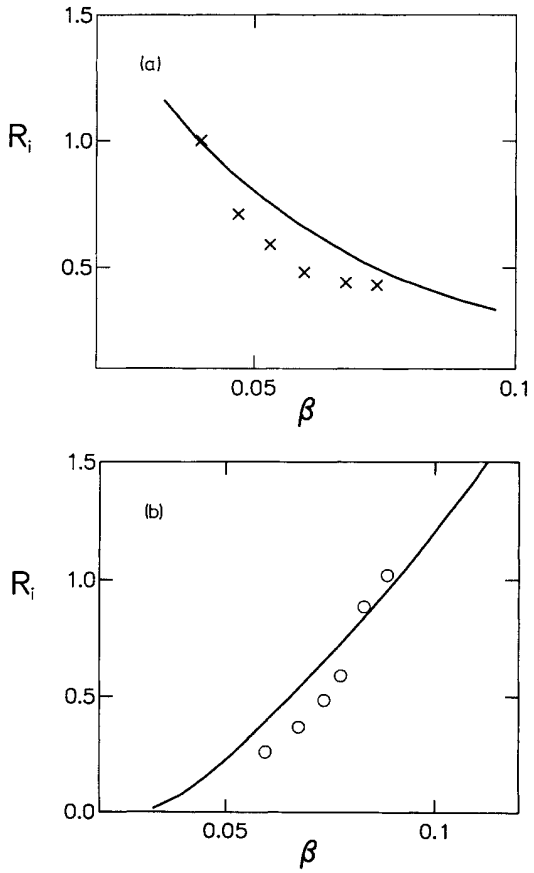

FIG. 9. Values of the activation energies R_i measured (crosses) as functions of β for the analog electronic circuit model of (3) with $\eta^2 = 0.033$ for (a) R_1 and (b) R_2. The curves are the numerical data of Fig. 3(a).

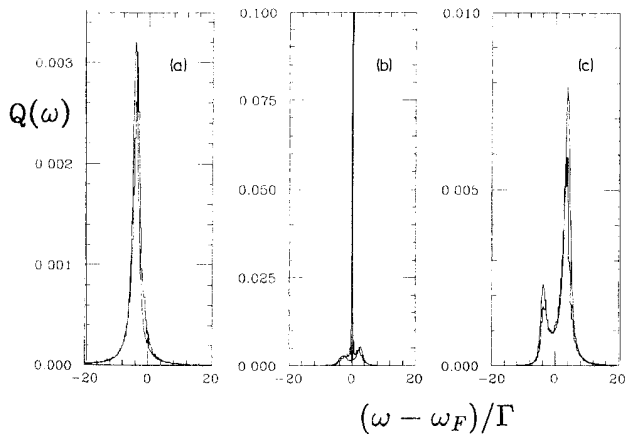

FIG. 10. Spectral densities $Q(\omega)$ of fluctuations measured (histograms) for the analog electronic circuit model of (3) with $\eta = 0.219$ and $\alpha = 8.69 \times 10^{-2}$ for (a) $\beta = 0.048$, (b) $\beta = 0.078$, and (c) $\beta = 0.150$. The full curve represents the theory.

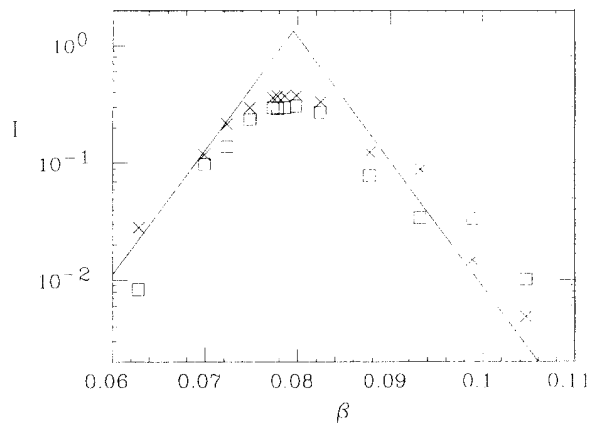

FIG. 11. Variation of the intensity I of the supernarrow spectral peak with distance from the kinetic phase transition line, measured as a function of β for the analog electronic circuit model of (3) for $\eta = 0.219$ and $\alpha = 8.69$ x 10^{-2}. The squares represent direct measurements; the crosses are derived from (21), based on measured transition rates. The full lines also represent (21), but for $\ln(w_1 w_2)$ given by (31) with measured R_1', R_2'.

ments refer to the spectral density of *fluctuations about an ensemble average*; the subtraction of $\langle q(t) \rangle$ from each realization $q(t)$ prior to computation of $Q(\omega)$ ensures that, when the system remains on one particular attractor throughout, most of the δ-function-shaped peak at ω_F [which is the Fourier transform of $\langle q(t) \rangle$] gets removed. This is why there is very little sign of a spectral peak at ω_F in Figs. 10(a) and 10(c). In the KPT range, however, where jumping occurs between the attractors, the general appearance of the spectrum is entirely different. In fact, the most striking feature of the spectrum is the supernarrow peak [15] that rises in the phase-transition range, where $\beta \simeq \beta_0(\eta)$, as seen in Fig. 10(b). Its width is very much smaller than either of the widths of the other peaks, or the experimentally determined damping constant Γ, or the frequency detuning $\omega_F - \omega_0$ (which are all of the same order of magnitude). For small noise intensities α, this width is unresolved by the LAB80 data-analysis system, i.e., the peak lies entirely within one "bin" of the data processor's memory. It was necessary to increase the noise intensity substantially in order to spread the peak over two or three bins.

The dependence of the intensity I of the supernarrow peak on the distance from the phase transition line was found to be exponential, as shown in Fig. 11. This feature can readily be understood in terms of (2), (15), and (21). According to (21), for small noise intensities where $\langle u_i \rangle \simeq u_i$,

$$I = \int_{-\infty}^{\infty} d\omega Q_{\rm tr}(\omega) = \frac{2\omega_F |\omega_F - \omega_0|}{3|\gamma|} |u_1 - u_2|^2 w_1 w_2 \ . \tag{30}$$

Not too far from, but not too close to, the phase-transition line where, on the one hand, $|\beta - \beta_0(\eta)| \ll 1$ and, on the other, the transition probabilities W_{12} and W_{21} differ substantially from each other, the coefficient $w_1 w_2$ in (21) should behave, according to (2), (15) as

$$w_1 w_2 \propto \exp\{-|R_1' - R_2'||\beta - \beta_0(\eta)|/\alpha\} \ , \tag{31}$$

where $R_i' = (\partial R_i/\partial\beta)_{\beta=\beta_0(\eta)}$. Therefore, the dependence of I on $(\beta - \beta_0)$ should indeed be exponential. In the immediate vicinity of the phase transition, where the exponent on the right hand side of (31) is of order unity, this exponential dependence will be smeared. Such smearing is clearly seen in the experimental data (squares in Fig. 10), which are in good agreement with (30) as indicated by the crosses (w_1, w_2 having been taken from independent measurements of the transition probabilities). Agreement with (30) based on $w_1 w_2$ taken from the simple estimate (31), as indicated by the full lines, is also good: the values of $R_{1,2}'$ in this case were taken from the slopes of the experimental $R_{1,2}(\beta)$ measurements and the prefactor in (31) was taken to be $\frac{1}{4}$ so as to give the correct maximum value of $w_1 w_2$ at the phase transition point $\beta = \beta_0(\eta)$ in the limit $\alpha \to 0$. The cusplike dependence of the intensity I of the supernarrow peak in the SDF is a characteristic feature of the peak, which itself represents a characteristic phase-transition phenomenon peculiar to bistable systems.

For β, η lying far from the phase transition line $\beta_0(\eta)$, the supernarrow peak is not seen, but there remain (histograms of Fig. 10) the much broader and less intense peaks in the SDF corresponding to fluctuations about the stable states. These correspond to the partial spectra of the first term in (18) and are well described (full curves) by (19). The characteristic feature is that they each ($j = 1, 2$) display a twin-peaked structure for a certain range of parameters. It can be seen from (19) that such structure should be at its most pronounced for the spectrum $Q_j(\Omega)$ when $|\nu_j| \gg 1$, that is, for sufficiently large frequency detuning $|\omega_F - \omega_0| \gg \Gamma$. Under these conditions, the peaks appear at $(\omega_F - \omega_0) \simeq \pm\Gamma\nu_j$, and their half width $\sim \Gamma$ is small compared to the distance separating them. The twin-peaked structure can be understood intuitively in terms of the forced vibrations at frequency ω_F in a given stable state being modulated by

the relatively slow (characteristic frequency $\sim \omega_F - \omega_0$) fluctuational vibrations about this state. We notice that the intensities of the peaks in a doublet differ markedly (parametrically strongly, in the case of the small amplitude attractor), so that the intensity of the second peak for the small amplitude attractor is fairly small.

In the range of the kinetic phase transition, the partial spectra $Q_1(\omega), Q_2(\omega)$ are superimposed and the supernarrow peak is also present. Thus there can be up to five separate peaks in the spectrum. A multipeaked structure is clearly evident in the results of Fig. 12, which were recorded for a larger detuning and a smaller Γ. A satisfactory quantitative description of such a spectrum cannot, however, be arrived at on the basis of (19), because it is significantly influenced by higher-order terms in the noise intensity, i.e., by vibrations at the overtones of $\Gamma\nu_j$, that were ignored in the derivation of (19). A detailed investigation of such higher-order effects is currently being planned and will be the subject of a future paper.

C. High-frequency stochastic resonance

In searching for evidence of the predicted HFSR phenomenon, the circuit parameters were initially set to $2\Gamma = 0.0397$, $\omega_0 = 1.00$, $\gamma = 0.1$, $\omega_F = 1.072\,00$, $\Omega = 1.070\,97$, $F = 0.068$, and $A = 0.006$ (these values apply to Figs. 14 and 16 below). The frequencies of the additional weak trial force and the main periodic drive were therefore very close to each other. A typical SDF, measured for a $16k$ digitized time series in the memory of the Nicolet 1280 data processor with input noise intensity $B = 0.040$, is shown in Fig. 13. The central maximum is the supernarrow SDF peak of Fig. 10(b), here with its finite width clearly resolved (note the highly expanded abscissa scale). A δ-function spike is evident, not only at Ω, but also at the mirror-reflected frequency $(2\omega_F - \Omega)$ just as predicted in Sec. II C.

The signal strengths (integrated intensities) $S(\alpha)$,

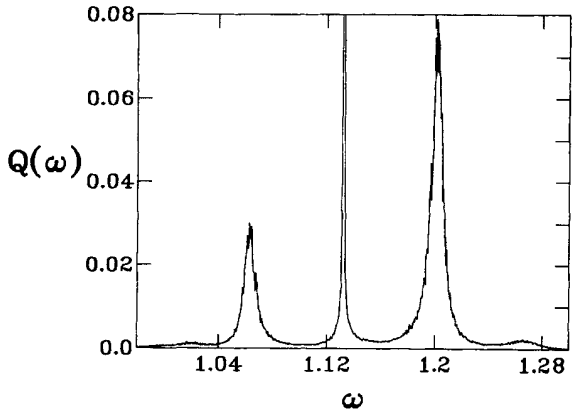

FIG. 12. An example of the kind of multipeaked spectral density of fluctuations $Q(\omega)$, measured in the range of the kinetic phase transition for the analog electronic model of (3), with relatively large frequency detuning and small damping. The parameters are $\eta = 0.055$, $\beta = 0.0303$, $\Gamma = 0.0073$, and $\alpha = 0.238$. Five spectral peaks — the supernarrow peak and four peaks of the partial spectra — are clearly resolved.

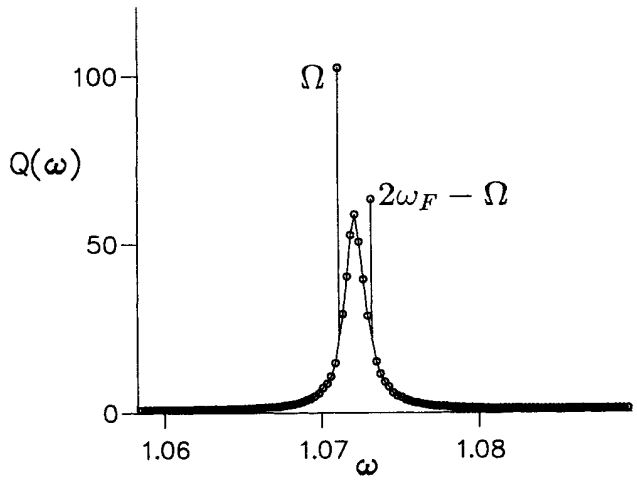

FIG. 13. Spectral density $Q(\omega)$ of the fluctuations of (3) as a function of frequency ω with an additional weak periodic (trial) force $A\cos(\Omega t + \phi)$ added on the right hand side, measured for the analog electronic circuit model. The contents of each FFT memory address are shown as a separate data point on a highly expanded abscissa (unscaled experimental unit). A smooth curve has been drawn through the background spectrum (the supernarrow peak, which has its maximum at ω_F) as a guide to the eye; vertical lines indicate the δ spikes resulting from the trial force.

$\mathcal{S}(\alpha)$, determined from measurements of the δ spikes, are plotted (data points) as functions of the reduced noise intensity $\alpha \propto B$ in Figs. 14(a) and 14(b). It is immediately apparent that there are well-defined maxima in the plots of $S(\alpha), \mathcal{S}(\alpha)$, thereby confirming the occurrence of HFSR in (3). The signal-to-noise ratio of P and $\mathcal{P}$ (i.e., the ratio of S and $\mathcal{S}$ to the "background" SDF in the absence of the trial force) has also been measured. As shown in Fig. 15, although the statistical quality of the data is somewhat poorer (owing to the additional error in the background SDF), there is no doubt that $P, \mathcal{P}$ each fall and rise and fall again with increasing noise intensity. The fall in $P, \mathcal{P}$ with increasing α at small α is, of course, a feature that is familiar from earlier calculations and experiments on conventional SR involving static bistable attractors; the signal-to-noise falls initially because, for very weak noise, the interattractor transitions are too rare to make significant contributions either to the susceptibility or to the SDF, whereas the background SDF in the denominator corresponding to fluctuations about the attractors steadily increases with noise intensity.

The theoretical predictions, based on Eqs. (18), (19), (21), (24)–(26), and (28), are shown by the full curves in Figs. 14 and 15. The agreement is not perfect, but (given the problem with the determination of β; see Sec. III) it is within the experimental error and may be regarded as satisfactory. The onset of the observed rise in $S, \mathcal{S}, P, \mathcal{P}$ occurs at the value α_0 of noise intensity for which the width of the supernarrow peak in the SDF becomes comparable with the frequency difference $|\Omega - \omega_F|$ (provided that the latter is not itself exponentially small; cf. [5(b)] where the position of the minimum of the SNR versus noise intensity has been discussed for stochastic

resonance in a system fluctuating in a static bistable potential). It is the increasing role of fluctuational transitions that is responsible for high-frequency stochastic resonance. These results, and the good agreement obtained with the theory of Sec. II, demonstrate that HFSR for periodic attractors may be perceived as a linear response phenomenon, in very close analogy to conventional SR for a static bistable potential [5].

An intuitive understanding of the mechanism of HFSR can be gained by recalling that, under the conditions considered here with $|\Omega - \omega_F|$ very small, the system responds to the trial force almost adiabatically. In terms of the phase diagram Fig. 1, the beat envelope of the combined main and trial periodic forces results in a slow vertical oscillation of the operating point p. When this is set (see line p'-p-p'') to straddle the KPT line, which was the case for present investigations, and the noise intensity is in the appropriate range, the system will have a tendency to make interattractor transitions *coherently*, once per half cycle of the beat frequency. The net effect is to increase the modulation depth of the beat envelope of the response, thereby amplifying its component frequencies Ω and $|\Omega - 2\omega_F|$.

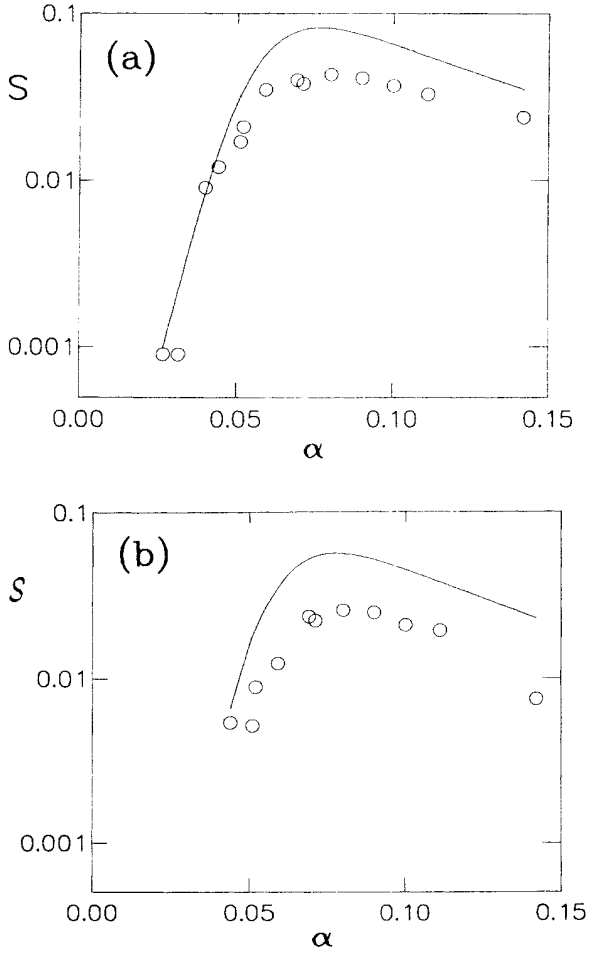

FIG. 14. The intensities S and $\mathcal{S}$ of the δ-shaped peaks in the SDF of the analog electronic model of (3) (data points) with $\beta = 0.103$ and $\eta = 0.266$ induced by a weak trial force $A\cos\Omega t$, plotted as a function of noise intensity α, compared with theory (full curves) (a) at the trial force frequency Ω and (b) at the mirror-reflected frequency $(2\omega_F - \Omega)$.

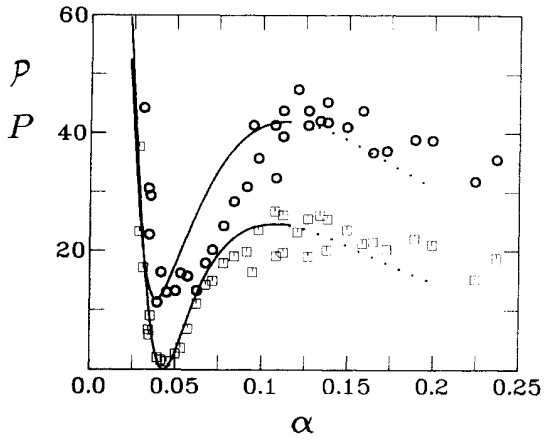

FIG. 15. The signal-to-noise ratios P and $\mathcal{P}$ of the responses at $\beta = 0.0814$ and $\eta = 0.236$ to the trial force at frequencies Ω (circle data and associated curve) and $(2\omega_F - \Omega)$ (squares), measured as functions of noise intensity α for the analog electronic circuit model of (3). The curves represent the theory. For noise intensities near those of the maxima in $P(\alpha)$, $\mathcal{P}(\alpha)$, the asymptotic theory is only qualitative and so the curves are shown dotted.

The magnitude of the signal at Ω has been measured as a function of distance, expressed in terms of β, from the KPT. The result is shown in Fig. 16. It exhibits a fast cusplike (note the log scale) decrease of S as β moves away from its critical value, demonstrating that, like the associated supernarrow spectral peak (see Sec. IV B), HFSR for periodic attractors has the character of a critical phenomenon, in agreement with the theory of Sec. II.

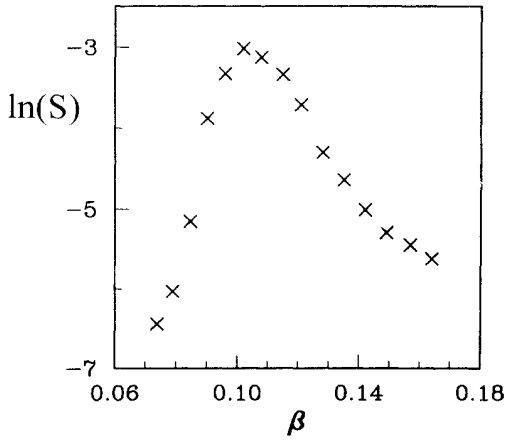

FIG. 16. Dependence of the logarithm of the intensity S of the spectral peak induced by the trial force for the analog electronic circuit model of (3) at a fixed noise intensity $\alpha = 0.076$, plotted as a function of β, varying across the KPT line.

V. CONCLUSION

Studies of a very simple nonequilibrium bistable system — a nearly resonantly driven nonlinear oscillator — have enabled us to observe and investigate a number of phenomena of rather general applicability and, in doing so, to test a theoretical approach to the calculation of transition probabilities in noise-driven nonequilibrium systems. The onsets of the supernarrow peak in the spectral density of the fluctuations and the corresponding peak in the susceptibility, and the phenomenon of high-frequency stochastic resonance, can all be viewed as examples of critical kinetic phenomena in periodically driven systems. They may be used not only to investigate the character and properties of kinetic phase transitions (as here), but also to obtain tunable noise-induced amplification of the signal-to-noise ratio and extremely narrowband filtering and detection of high-frequency signals.

Finally, it is interesting to note that many of the phenomena discussed above provide illustrations of the *creative* role often played by noise in nonlinear systems. The occurrence of the extremely strong and highly selective four-wave mixing, for example, arises because of the noise and does not occur in the absence of noise; the dependences on noise intensity both of this effect, and of the other critical phenomena discussed in the present paper, are exponentially sharp.

ACKNOWLEDGMENTS

Two of us (M.I.D. and D.G.L.) acknowledge the extremely warm hospitality of Lancaster University, where this work was done during their visits. The research was supported by the Science and Engineering Research Council (U.K.), by the Royal Society of London, and by the European Community.

APPENDIX

The calculation in [3] of transition probabilities for systems driven by Gaussian noise implied an idea [25] due to Feynman. His suggestion was that there was a direct relationship between the probability density of the paths of the noise-driven system and the noise itself. This interrelationship allows us to write immediately, to logarithmic accuracy, the probability density functional for the paths of the system and to set up the variational formulation giving the most probable paths for first reaching a given point in the phase space of the system and for the transitions between the stable states (see also Ref. [2]). In the white noise case under consideration, the "activation energy" R_j characterizing the transition of the oscillator from the stable state j to the stable state i is given [3] by the following variational problem:

$$R_j = \frac{1}{4}\eta^{-2}\min\int_{-\infty}^{\infty} d\tau \left(\frac{du}{d\tau} - v\right)\left(\frac{du^*}{d\tau} - v^*\right) , \tag{A1}$$

$$v \equiv v(u,u^*), \qquad u(-\infty) = u_j, \qquad u(\infty) = u_s,$$

where v is defined by (6) and u_j and u_s are the values of the "slow" variable u for the initially occupied stable state and for the saddle point, respectively. The general analysis of large occasional fluctuations in systems driven by white noise was given by Wentzell and Freidlin [26].

In obtaining a variational (Euler) equation for the problem (A1), u and u^* should be varied independently. The resulting equation can be seen to be of the form

$$\frac{d^2u}{d\tau^2} - 2i\frac{du}{d\tau}(2|u|^2 - 1) - \eta^2 u\nu^2 + \sqrt{\beta}(2|u|^2 + u^2 - 1 - i\eta) = 0 , \tag{A2}$$

$$\nu^2 \equiv \nu^2(u,u^*) = 1 + \eta^{-2}(|u|^2 - 1)(3|u|^2 - 1)$$

together with the equation for u^* complex conjugate to (A2). The corresponding equations for $u' \equiv \mathrm{Re}u$ and $u'' = \mathrm{Im}u$ were written down explicitly in Ref. [3]. An analytic solution can be obtained [3] in some limiting cases. The equations (A2) describe the conservative motion of an auxiliary system with two degrees of freedom, its coordinates being u' and u'' and its velocities $\dot{u}'$ and $\dot{u}''$. The motion can be considered as the planar motion of a particle of unit mass and unit electric charge in an electric potential

$$U(u',u'') = -\frac{1}{2}\left(\frac{\partial g}{\partial u''} + \eta u'\right)^2 - \frac{1}{2}\left(\frac{\partial g}{\partial u'} - \eta u''\right)^2 , \tag{A3}$$

where

$$g(u',u'') = \frac{1}{4}(u'^2 + u''^2 - 1)^2 - u'\sqrt{\beta}$$

and a magnetic field $\mathcal{H} = [4(u'^2 + u''^2) - 2]$ normal to the plane. The potential $U(u',u'')$ is shown in Fig. 17. It has three maxima of equal height (=0). They correspond respectively to the stable states and the unstable stationary state of the system. Note that we are dealing with the *auxiliary* system. Thus, not minima, but maxima of the potential $U(u',u'')$ correspond to the stable states of the initial system (a circumstance typical of the instanton-type formulation that we are using). The problem (A1) amounts to finding a path that starts on one of the outer maxima and arrives at the maximum corresponding to the saddle point.

The numerical solution in the general case of arbitrary values of (β,η) can be simplified by the following procedure (cf. [27]). Near the stable state j, when $|u-u_j| \ll 1$, Eq. (A2) can be linearized in $u-u_j, u^*-u_j^*$. The solution can then be sought in the form

$$u(\tau) - u_j = \sum_s A_j^{(s)}\exp(\lambda_j^{(s)}\tau) , \tag{A4}$$

$$u^*(\tau) - u_j^* = \sum_s B_j^{(s)}\exp(\lambda_j^{(s)}\tau)$$

for $\tau \to -\infty$, with

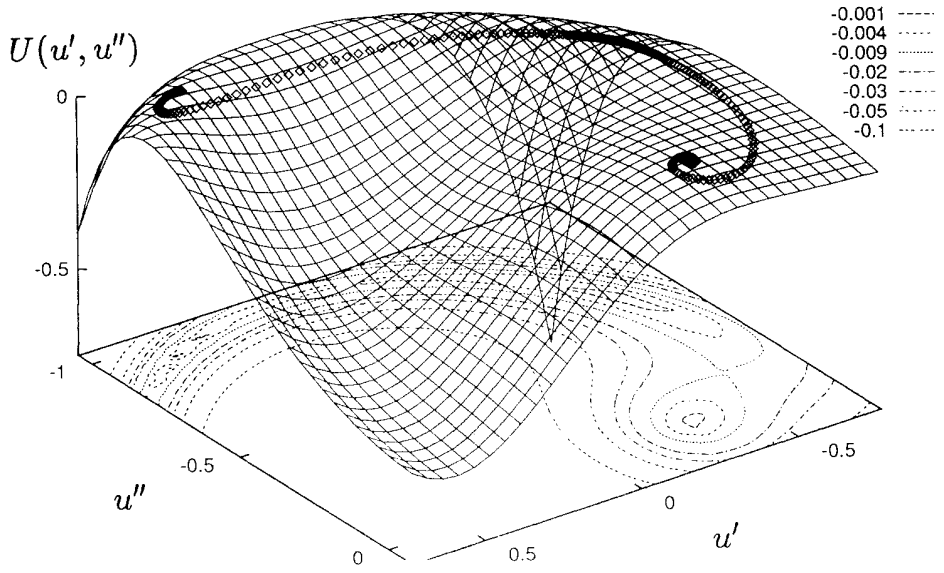

FIG. 17. The three-humped potential $U(u', u'')$ of Eq. (A3) for the auxiliary system, portrayed both as a three-dimensional surface and, below it, in the form of a contour plot; the contour altitudes are tabulated on the right hand side. (Note, however, that the left hand potential maximum is so shallow that it is barely visible in the contour plot.) The optimal path of the escape from the focus-1 (the small amplitude attractor) is shown by the line of $\diamond$ points. It goes from this focus (the right hand potential maximum) to the saddle point (central maximum). On its way from the saddle point to the focus-2 (the left-hand potential maximum corresponding to the large amplitude attractor) the system moves, with overwhelming probability, along the noise-free path. The $\diamond$ points are equally spaced in time, so that the speed with which the system is traveling along different elements of the path may be inferred from the density of the points; it moves most slowly at the three potential maxima. The values of the dimensionless parameters for the plot were $\eta^2 = 0.072$ and $\beta = 0.104$.

$$B_j^{(s)} = A_j^{(s)} \frac{\lambda_j^{(s)2} - 2i\lambda_j^{(s)}(2|u_j|^2 - 1) - (\eta^2 + 5|u_j|^4 - 4|u_j|^2 + 1)}{2u_j^2(2|u_j|^2 - 1 - i\eta)} . \tag{A5}$$

The resultant characteristic equation gives four values for the increment λ

$$\lambda_j^{(1,2)} = \alpha_j^{(1,2)}, \quad \lambda_j^{(3)} = -\alpha_j^{(1)}, \quad \lambda_j^{(4)} = -\alpha_j^{(2)} , \tag{A6}$$

where $\alpha_j^{(1,2)}$ are the roots of the characteristic equation for the motion of the oscillator in the vicinity of the state j in the absence of the random force (the latter being described by the linearized equation $du/d\tau = v$),

$$\alpha_j^{(1,2)} = -\eta[1 \pm i(\nu_j^2 - 1)^{\frac{1}{2}}], \quad \nu_j^2 \equiv \nu^2(u_j, u_j^*) . \tag{A7}$$

For the stable state, $\mathrm{Re}\alpha_j^{(1,2)} < 0$; note that this implies that $\nu_j^2 > 0$.

It is evident from (A4)–(A7) that the coefficients $A_j^{(1,2)}$ (and thus $B_j^{(1,2)}$) in (A4) should be set equal to zero; otherwise, the path $u(\tau)$ will not approach u_j as $\tau \to -\infty$. At this point we have arrived at two independent parameters in (A4): $A_j^{(3)}$ and $A_j^{(4)}$. However, it is their *ratio* which determines the direction in which the system will move along the extreme path (A2); accordingly, it is this ratio that should be determined from the boundary conditions $u(\infty) = u_s$ (A1). We thus obtain an implicit equation for the single quantity $A_j^{(3)}/A_j^{(4)}$. It can in principle be solved numerically by a shooting method (cf. [28]). This method works most effectively for small damping $\eta \ll 1$, when the optimal path $u'(\tau), u''(\tau)$ is a spiral.

Here we adopt a relaxation method [29]. The differential equations are cast in the form of nearest neighbor difference equations. The boundary values of u, u^* were chosen at u_j, u_s. (The results were the same to the adopted accuracy when u_{3-j} was taken instead of u_s, i.e., the optimal path for the escape from the state j was supposed to start from u_j and to arrive at the other stable position u_{3-j}; moreover, it turned out that the path found in this way passed through, or fairly close to, the saddle point.) A guess at the solution was tried and then it was successively improved by assuming, at each step, that the true solution was close to the current one and linearizing about the latter. Even for fairly different initial guesses, the same final solution $u(t)$ was obtained, implying that the method is reliable. The same results were obtained for different integration times, which were always very large compared to the characteristic dimensionless times $\sim 1, \eta^{-1}$, in (A2).

Solutions were used to compute the action integral (A1). The results are summarized in Fig. 17. The op-

timal path is indicated by the diamond points, which are separated by equal intervals of time. The motion is naturally at its slowest (points closest together) on the maxima of the potential; because of the effect of the "magnetic field" $\mathcal{H}$, it does not pass *exactly* along the ridges. The advantage of the relaxation method is that it is fairly fast and convenient. On the other hand, for small η where the optimal path is a small-step spiral, it is less reliable than the method based on solving Eqs. (A4)–(A7) which was used in [28].

When, in addition to the strong field $F\cos\omega_F t$, the oscillator is also driven by a weak force $A\exp(-i\Omega t)$, the expressions for R_j will change. The additions to R_j can readily be found when $|\Omega-\omega_F|\ll\Gamma$, because the characteristic time of the motion along the extreme path described by (A2) is Γ^{-1} (i.e., η^{-1} in dimensionless units of τ); thus, when $|\Omega-\omega_F|\ll\Gamma$, the weak field is not changed while the system is moving along the path. It is evident from (22) that the functional which should be minimized to give R_j in the presence of the field A is given by (A1) with v^* having been replaced by $v^*+i\tilde{A}(\tau)$. To first order in A, the change in R_j is thus of the form

$$\delta R_j(\tau) = \mu_j\tilde{A}(\tau), \quad \mu_j = -\frac{i}{4}\eta^{-2}\int_{-\infty}^{\infty}d\tau\left(\frac{du}{d\tau}-v\right), \tag{A8}$$

where the integral giving μ_j is calculated along the extreme path for $A=0$.

The expression for μ_j can be substantially simplified if one notices that the activation energy R_j (A1) is unchanged when $\beta^{\frac{1}{2}}$ is replaced by $\beta^{\frac{1}{2}}\exp(i\psi)$ in (6) and (A1) respectively, where ψ is arbitrary: such a replacement corresponds simply to a shift of the time origin in (5) by ψ/ω_F, which should not influence stationary characteristics of the oscillator such as R_j. By differentiating R_j with respect to ψ for $\psi\to 0$, one finds immediately that $\mathrm{Im}\mu_j=0$, and it is then easy to see that

$$\mu_j = \sqrt{\beta}\,\partial R_j/\partial\beta\,. \tag{A9}$$

[1] H. A. Kramers, Physica **7**, 284 (1940).

[2] M. I. Dykman and K. Lindenberg, in *Some Problems in Statistical Physics*, edited by G. Weiss (SIAM, Philadelphia, 1994).

[3] (a) M. I. Dykman and M. A. Krivoglaz, Zh. Eksp. Teor. Fiz. **77**, 60 (1979) [Sov. Phys. — JETP **50**, 30 (1979)]; (b) in *Soviet Physics Reviews*, edited by I. M. Khalatnikov (Harwood Academic, New York, 1984), Vol. 5, p. 265.

[4] M. I. Dykman, R. Mannella, P. V. E. McClintock, F. Moss, and S. M. Soskin, Phys. Rev. A **37**, 1303 (1988).

[5] (a) M. I. Dykman, P. V. E. McClintock, R. Mannella, and N. G. Stocks, Pis'ma Zh. Eksp. Teor. Fiz. **52**, 780 (1990) [JETP Lett. **52**, 141 (1990)]; M. I. Dykman, R. Mannella, P. V. E. McClintock, and N. G. Stocks, Phys. Rev. Lett. **65**, 2606 (1990); (b) *ibid.* **68**, 2985 (1992).

[6] R. Benzi, A. Sutera, and A. Vulpiani, J. Phys. A **14**, L453 (1981); C. Nicolis, Tellus **34**, 1 (1982); R. Benzi, G. Parisi, A. Sutera, and A. Vulpiani, *ibid.* **34**, 10 (1982).

[7] B. McNamara, K. Wiesenfeld, and R. Roy, Phys. Rev. Lett. **60**, 2626 (1988); R. F. Fox, Phys. Rev. A **39**, 4148 (1989); B. McNamara and K. Wiesenfeld, *ibid.* **39**, 4854 (1989); Hu Gang, G. Nicolis, and C. Nicolis, *ibid.* **42**, 2030 (1990); M. I. Dykman, G. P. Golubev, D. G. Luchinsky, A. L. Velikovich, and S. V. Tsuprikov, Pis'ma Zh. Eksp. Teor. Fiz. **53**, 182 (1991) [JETP Lett. **53**, 193 (1991)].

[8] For a fuller bibliography and reviews of the rapidly expanding field of stochastic resonance, see the special issue of J. Stat. Phys. **70**, Nos. 1/2 (1993), and the papers and references therein.

[9] H. M. Gibbs, *Optical Bistability: Controlling Light with Light* (Academic, New York, 1985).

[10] L. D. Landau and E. M. Lifshitz, *Mechanics* (Pergamon, London, 1976).

[11] G. Gabrielse, H. Dehmelt, and W. Kells, Phys. Rev. Lett. **54**, 537 (1985).

[12] M. I. Dykman, M. A. Krivoglaz, and S. M. Soskin, in *Noise in Nonlinear Dynamical Systems*, edited by F. Moss and P. V. E. McClintock (Cambridge University Press, Cambridge, England, 1989), Vol. 2, p. 347.

[13] M. I. Dykman, R. Mannella, P. V. E. McClintock, and N. G. Stocks, Phys. Rev. Lett. **65**, 48 (1990).

[14] B. A. Huberman and J. P. Crutchfield, Phys. Rev. Lett. **43**, 1745 (1979).

[15] See, for example, J. M. T. Thompson and H. B. Stewart, *Nonlinear Dynamics and Chaos* (Wiley, New York, 1987), and references therein.

[16] F. T. Arecchi, R. Badii, and A. Politi, Phys. Rev. A **32**, 402 (1985).

[17] N. N. Bogolyubov and Yu. A. Mitropolsky, *Asymptotic Methods in the Theory of Nonlinear Oscillators* (Gordon and Breach, New York, 1961).

[18] M. I. Dykman and V. N. Smelyanskiy, Phys. Rev. A **41**, 3090 (1990).

[19] R. Bonifacio and L. A. Lugiato, Phys. Rev. Lett. **40**, 1023 (1978); L. A. Lugiato, Prog. Opt. **21**, 69 (1984).

[20] L. D. Landau and E. M. Lifshitz, *Statistical Physics*, 3rd ed. (Pergamon, New York, 1980), Pt. 1.

[21] Stochastic resonance was originally considered (see Ref. [6]) just as a periodic-field-induced periodic redistribution over the stable states.

[22] Y. R. Shen, *The Principles of Nonlinear Optics* (Wiley, New York, 1984).

[23] L. Fronzoni, in *Noise in Nonlinear Dynamical Systems* (Ref. [12]), Vol 3, p. 222; P. V. E. McClintock and F. Moss, *ibid.* p. 243.

[24] P. Hänggi, T. J. Mroczkowski, F. Moss, and P. V. E. McClintock, Phys. Rev. A **32**, 695 (1985).

[25] R. P. Feynman and A. R. Hibbs, *Quantum Mechanics and Path Integrals* (McGraw-Hill, New York, 1965).

[26] A. D. Wentzell and M. I. Freidlin, Russ. Math. Surveys **25**, 1 (1970); M. I. Freidlin and A. D. Wentzell, *Random Perturbations of Dynamical Systems* (Springer, New York, 1984).

[27] D. Ludwig, SIAM Rev. **17**, 605 (1975).

[28] V. A. Chinarov, M. I. Dykman, and V. N. Smelyanskiy, Phys. Rev. E **47**, 2448 (1993).

[29] W. H. Press, B. P. Flannery, S. A. Teukolsky, and W. T. Vetterling, *Numerical Recipes* (Cambridge University Press, Cambridge, England, 1986).